A&A manuscript no.
(will be inserted by hand later)
Your thesaurus codes are:
05. (05.01.1; 05.18.1; 10.19.2; 10.11.1)

ASTRONOMY
AND
ASTROPHYSICS
22.1.1996

Galactic structure along the main meridional section of the Galaxy. ⋆

I. The North Galactic Pole (N321) field

A. Spagna[1], M.G. Lattanzi[1,2], B.M. Lasker[2], B.J. McLean[2], G. Massone[1], and L. Lanteri[1]

[1] Osservatorio Astronomico, Strada Osservatorio 20,
I-10025 Pino Torinese, Italy
[2] Space Telescope Science Institute,
3700 San Martin Dr., Baltimore MD 21218, USA

Received 4 August 1995; accepted 5 December 1995

Abstract. This work presents the results of a new magnitude limited survey of colors (BVR_c) and proper motions in a new field at the North Galactic Pole (NGP), with extent $4^\circ \times 5^\circ$ and centered at ($l \simeq 162^\circ$, $b \simeq 87^\circ$). The plate material, digitized at the Space Telescope Science Institute, is from sky surveys taken with the Oschin Schmidt telescope on Palomar Mountain: POSS I, Quick-V and, for the first time, POSS II.

We provide V, $(B-V)$, $(V-R_c)$ photographic photometry for a stellar sample down to $V = 18.5$ with an accuracy of about 0.1 mag. Proper motions are on an absolute reference frame based on external galaxies, and their mean (total) internal error is about 3 mas/yr.

The procedures for the astrometric reduction and for the photometric calibration are described in detail, with emphasis on the techniques for the detection and the removal of systematic errors. External checks have been performed with independent astrometric and photometric catalogs. A comparison with the Lick NPM1 catalog shows an offset of about 4 mas/yr in μ_α, which does not seem to be due to the different procedures adopted in establishing the absolute frame.

Photometric parallaxes and galactic U,V velocities have been derived adopting a statistical model for the chemical effect based on a vertical metallicity gradient of $\partial[\mathrm{Fe/H}]/\partial z = -0.3$ Kpc^{-1}.

The subsample of stars with $4.5 \le M_V \le 5.0$ has been analyzed in order to investigate the vertical density distribution up to $z \approx 5000$ pc; a least squares decomposition of the vertical volume density with exponential density laws has converged to a thin disk with scale height of $z_0 \simeq 259 \pm 12$ pc and a thick disk with $z_0 \simeq 1137 \pm 61$ pc and a density $\rho_{0,\mathrm{thick}}$ 23 times smaller than $\rho_{0,\mathrm{thin}}$.

Mean V velocities (along with their dispersion) have been tabulated as function of distance, and the asymmetric drift is seen with outstanding clarity. A direct deconvolution of the histogram, assuming Gaussian-like distributions for each component, requires the presence of a halo with a rotation lag of -225 Km/s with respect to the Sun, and an intrinsic velocity dispersion of 140 Km/s.

Finally, a set of 28 stars with similar kinematics at an average distance of 4400 pc has been isolated, which, if confirmed, would support the existence of kinematically homogeneous non-thermalized groups within the population of the extended galactic disk.

Key words: astrometry – photometry – galaxy: structure – galaxy: kinematics and dynamics

1. Introduction

During a “golden” age which spanned the first decades of this century and which produced the classical works of Lindblad and Oort, the study of the stellar content of the Milky Way was essentially restricted to the solar neighbourhood. At the same time, our knowledge of galactic structure, based on complementary studies of extragalactic systems, developed rapidly. Since the 1970s, the availability of powerful modern tools such as automated plate scanning machines and computers has supported both fast impersonal analysis and massive data storage. The consequent strong stimulus to the study of the Galaxy has been resulting in the discovery of new structures and details that contribute to a more complete description of the

Send offprint requests to: spagna@to.astro.it

⋆ This work is based in part on the thesis of AS, presented in partial fulfillment for the Ph.D. degree of the University of Turin.

Milky Way and that furnish information on the physical processes that rule galactic dynamics.

Actually, if we confine ourselves simply to stellar populations, the Galaxy is already a very complex system. As a first approximation, such a system can be described by three main components: the spheroidal population (including the bulge and the halo), the thick/extended disk, and the thin disk, each with its own characteristic spatial distribution and kinematical and chemical properties[1].

An understanding of the physical parameters of these components can constrain our theoretical models of galactic formation and evolution. At the moment, only the thin disk parameters are known with adequate accuracy, while the thick disk and the spheroid properties are affected by several uncertainties. Faint in-situ surveys, which directly detect the main stellar components (dwarfs) of the various structures where they predominate, are a powerful tool to explore the regions outside the solar neighbourhood, i.e., without using tracers whose selection could bias the results. Such surveys are performed, on a field-by-field basis, by analysis of several plates of various passbands and of different epochs; this provides multicolor star-counts and accurate proper motions. Then deriving distances and linear velocities, one can obtain a picture of galactic structure and kinematics.

Several surveys of colors and proper motions in the vicinity of the North Galactic Pole have been performed. Chiu (1980), Spaenhauer (1989), Reid (1990) and Majewski (1992), investigated the SA 57 field; and Soubiran (1992a) and Kharchenko et el. (1994), a region close to the globular cluster M3 ($b \simeq 80°$); Kharchenko et el. also investigated the F14 field ($b \simeq 87°$), which is part of the MEGA program (Einasto et al. 1985 and references therein). For other directions, Murray et al. (1986) published results towards the South Galactic Cap; and intermediate latitude surveys have been presented by Evans (1988) and by Ojha et al. (1994a, 1994b) ($b \simeq 47°$).

In this paper we initiate the study of twelve fields selected along the meridian toward the galactic anticenter. This program is being performed in conjunction with the creation of the second-generation, all-sky Guide Star Catalog (GSC II) (Lasker 1992; Lattanzi 1993; Lasker, et al. 1995), which is based on the scan archive of the Space Telescope Science Institute (ST ScI). These scans are of the sky surveys from the Palomar and the UK Schmidt telescopes. By using the same observational material and reduction procedures as those being developed for the GSC II, we intended to serve as a demonstration of the feasibility of the GSC II and, recalling that the GSC II will include positions, proper motions and colors of $\approx 10^8$ stars, as a measure of its scientific potential for studies in galactic structure.

[1] See Gilmore et al. (1989) and Majewski (1993) for recent reviews.

Initially, we have derived colors and proper motions in two fields: a $4° \times 5°$ area close to the North Galactic Pole (NGP) ($b \simeq 87°$), and a $1\overset{\circ}{.}8 \times 1\overset{\circ}{.}8$ area on the galactic plane ($b \simeq 0°$) around the open cluster Stock2 (Spagna et al. 1996b). Here, we present details of the reduction techniques adopted for the project and give new results for the NGP field. To allow for a more direct understanding of the data, we opted for a mostly heuristic analysis, as opposed to direct comparisons with galaxy models.

2. Photographic material

This survey is based exclusively on existing survey plate material taken with the Oschin Schmidt telescope (Tab. 1) on Palomar Mountain. To the best of our knowledge, this is the first galactic structure work to integrate successfully plates from the new Palomar survey (POSS II), the 1950 survey (POSS I), and the so called Quick-V survey, which was made by the Palomar Observatory and the Space Telescope Science Institute (ST ScI) for the construction of the Guide Star Catalog (Lasker et al. 1990). Anticipating on the discussion below, we note here the outstanding astrometric potential of the two POSS II J and F plates used in this work; this of course is a consequence of low granularity of their (type IIIa) emulsions.

All plates were digitized at ST ScI, with PDS-type scanning machines (Lasker et al. 1990). The POSS I and Quick-V plates were scanned with a 25 μm pixel-size, corresponding to $1\overset{''}{.}7$ at the scale of the telescope (67 arcsec/mm); and the POSS II images were digitized with a pixel-size of 15 μm, i.e., $1\overset{''}{.}0$/pixel.

2.1. Plate reduction

The digitized plates were initially analyzed by means of a prototype ST ScI software package which performed the *identification* of the objects on the plates and supplied *classification* attributes (star, galaxy, noise, etc.) based on the computed image-features of each identified object.

An estimate of the plate position, (x_{ij}, y_{ij}), of the i-th object on the j-th plate, is given by the density-weighted object center. This estimate was then improved by means of the centroider in ROBIN, a package for image processing by Lanteri (1996). The ROBIN centroider uses an analytical model of the Point Spread Function (PSF) based on a circular Gaussian function with a tilted background plane. Tests show that the average error of the positions fitted with ROBIN ($\sigma_{x,y} \simeq$ 0.12-0.13 pixel) is about two times better than that of the positions derived with the barycenter centroider ($\sigma_{x,y} \simeq$ 0.21-0.22 pixel; see Spagna 1995 and Lanteri 1995, for the details of the comparison).

The volume, v, of the fitted Gaussian is strictly correlated to the integrated photographic density of the stellar images. Therefore, for the *stellar* instrumental magnitude we adopted the quantity $p = -2.5 \log v + \mathrm{const}$. The lin-

Table 1. Plate material

Survey	*Plate*	α_c (J2000)	δ_c (J2000)	*Pixel*	*Epoch*	*Exposure*	*Band*	*Emulsion/filter*
POSS I	64-O	$12^h41^m\!.1$	$29°12'$	$1''\!.70$	1950.275	12 m	O	103a-O unfiltered
	64-E	$12^h41^m\!.1$	$29°12'$	$1''\!.70$	1950.275	45 m	E	103a-E + red plexiglass
Quick-V	N321	$12^h41^m\!.1$	$29°12'$	$1''\!.70$	1983.293	20 m	V_{12}	IIa-D + Wratten 12
POSS II	XJ442	$12^h41^m\!.2$	$29°45'$	$1''\!.00$	1990.225	75 m	J	IIIaJ+ GG385
	XP442	$12^h41^m\!.3$	$29°44'$	$1''\!.00$	1990.081	75 m	R_P	IIIaF + RG610

earization and calibration of the photometric index p is described in Sect. 4.

Table 2. Statistics of the identifications for the NGP images

Ref. plate	*No. of targets*					
N321	16436					
Plate	*No. of counterparts*					
	0	1	2	3	4	≥ 5
64-O	2766	14521	343	25	0	0
64-E	2223	14803	585	40	4	0
XJ442	2058	14087	1333	127	31	19
XP442	2005	13293	2082	245	25	5

2.2. Cross-identifications

The lists of positions, (x_{ij}, y_{ij}), and photometric indices, p_{ij}, from the different plates were matched using the intermediate epoch plate (Quick-V) as reference. After determining an approximate coordinate transformation to the reference plate, we looked for counterparts inside a search radius $r_0 = 12''$, which is typically small compared to the mean star separation, i.e., $\sim 130''$, i.e., on the assumption of a *uniform* distribution. This matching limit fixes the maximum detectable proper motion to $0''\!.39$/yr.

In Tab. 2, the statistics of the matches, including multiple identifications, are presented. In the magnitude range $9.5 \leq V \leq 18.5$, we have obtained a photometric catalog containing magnitudes and colors of 12 708 stars. The astrometric catalog with proper motions, for which we used the more stringent requirement of counterparts on *all* of the plates, contains 10 230 stars.

3. Faint photometric standards

Field N321 lacked published faint photometric sequences for the calibration of the photographic photometry. Accordingly, we obtained new CCD observations to establish sequences of standard stars in the BVR_c Johnson-Cousins photometric system, down to $V \simeq 19$ mag. Three fields, each $11'$ on a side, were imaged the night of June 5 1994 with the 1032 × 1032 pixel CCD at the Whipple Observatory 1.2 m telescope on Mt. Hopkins (scale $\simeq 0''\!.67$/pixel). The CCD fields were placed at the center, the North-East, and the North-West edges of the $4° \times 5°$ region investigated.

Transformation to the standard Johnson-Cousin system was done via the usual method of observing a set of primary photometric standard stars, those of Landolt (1991) in this case, at different air masses. The raw CCD frames were calibrated utilizing standard packages, i.e., bias subtractions and flat-field corrections with MIDAS (Grøsbol & Ponz 1985) and image centering and instrumental magnitudes with DAOPHOT 2.0 in MIDAS (Stetson 1987). The derivation of the transformation constants used a version of the code SNOPY developed at ESO, properly modified to run on CCD data (Mitton 1992). The precision of magnitudes and colors is typically better than 0.05 mag within the magnitude interval $9 \leq V \leq 19$.

The details on these standard photometric sequences are given in Spagna et al. (1996a); the data are available on request.

4. Photographic Photometry

4.1. Photometric accuracy

Several systematic corrections must be taken into account when performing photometric calibrations of large format Schmidt plates. The problem is that the CCD standard sequences covering only small areas, while the plate as a whole is affected by position dependent sensitivity variations. Geometric *vignetting* is known to exist and is amenable to empirical calibration. In principle, vignetting should cause only position-dependent variations in the zero point of the magnitude scale, with no effect on the slope of the calibration or on color. However, this is strictly true only for densities within the linear portion of the plate characteristic curve; outside of this regime, magnitude and color terms may be expected.

Another major source of position-dependent systematic errors is sensitivity variations across the plate; these are primarily due to non-uniformities in the emulsion and in the plate processing.

Finally, the extracted photometric parameters are subject to the variation of the stellar PSF with plate position and with color. This is a direct consequence of the fact that the photometric indices depend on the shape of this function and the effective wavelength of the plate-filter-star combination. PSF changes can result from reflections between filter and emulsion, diffraction by obstructions in

Table 3. Transformation to natural bandpasses

Transformation	*Color range*	*RMS*	*Reference*
$V_{12} = V - 0.15(B - V)$		-	Russell et al. 1990
$(O - B) = f(B - V)$			Humphreys et al. 1991
interpolation	$-0.3 \leq (B - V) \leq 1.46$	-	
extrapolation	$1.46 \leq (B - V) \leq 3.0$	-	
$E \simeq R_c$	$0.3 \leq (B - R_c) \leq 2.6$	0.115	Evans 1988
$J = B - 0.315(B - V) + 0.005$	$-0.4 \leq (B - V) \leq -0.05$	0.002	Majewski 1992
$J = B - 0.228(B - V) + 0.003$	$-0.05 \leq (B - V) \leq 1.5$	0.008	

the beam (the plate holder and its supports), and residual aberrations. Observational effects (e.g., differential refraction, guiding errors) also modify the shape of PSF. (Notice that PSF variations are important for astrometric centroiding as well.)

In what follows, we detail the procedures for the photometric calibration of the instrumental measures and for the detection and removal of the systematic errors.

4.2. Transformation to natural bandpasses.

The first step is to establish a sequence of reference magnitudes in the natural passband of the plates. This is accomplished using the B, V, R_c CCD data and published transformation equations (Tab. 3).

For the O band we have used the $(O - B) = f(B - V)$ relation of Humphrey et al. (1991). This relation has been extended to $(B - V) = 3$ by linear extrapolation of the published data redder than $(B - V) = 1.46$. For E and V_{12} bands, we have adopted the empirical equation $E \simeq R_c$, as derived by Evans (1988), and the relation $V_{12} = V - 0.15(B - V)$ from Russell et al. (1990, and references therein), respectively. Majewski (1992) provided the relation $J - B = f(B - V)$. He also gives the transformation $V - I_c \rightarrow R_P - R_c$ which we could not use for the lack of I_c photometry. Therefore, the transformation $R_P \approx R_c$ was assumed as an initial approximation.

4.3. Linearization of instrumental magnitudes

The generic model which relates instrumental magnitudes to the linear magnitude scale defined by a suitable set of reference magnitudes in a given natural bandpass can be written as:

$$m = f(p) + \epsilon(x, y), \tag{1}$$

where p is the instrumental magnitude derived from our object identification code (see Sect. 2.1), and ϵ is a correction term which depends on plate position and is assumed to vanish within the (relatively small) region occupied by the set of standard stars. The $\epsilon(x, y)$ is conceptually very important, and may be considered the photographic analogue of flat fielding used in CCD observing. It includes all the position-dependent effects addressed above.

On examining the post-fit residuals, we have found that an adequate choice for the function $f(p)$ is the Tsubaki-Engvold equation, which was originally developed for a somewhat different photometric application (see Lasker et al. 1990, and references therein):

$$m = \Phi_1 p + \Phi_2 \ln(e^{Bp^{C_1}} - 1) + \Phi_3 e^{Bp^{C_2}} + \Phi_4. \tag{2}$$

We adjusted only for the four linear parameters Φ_1 through Φ_4. The values of the constants C_1 and C_2 were kept at 1 and 0.7 respectively, while B was set to 0.01 to take into account the larger range spanned by the pseudo magnitude indicator adopted. The fitted function gives a photometric calibration spanning ~ 8 mag.

A direct evaluation of the correction term in Eq. (1) requires a uniform grid of suitable reference magnitudes covering the region of interest. In the near future, the availability of the TYCHO photometry may be expected to support such a calibration straightforwardly; however, for the present, a less direct, partial estimation of $\epsilon(x, y)$ is used.

The central and North-East CCD fields, about 2° apart in declination (approximately along the y-axis), were combined in one least squares solution for the evaluation of the model in Eq. (1). Before solving Eq. (1), the magnitudes of the *standards* were corrected for vignetting by means of the empirical formula $\Delta m_v(x, y)$ published in Russell et al. (1992) for the Oschin Schmidt[2]. The correction ϵ has been modeled as a linear effect in the y coordinate (the x-axis displacement of the two fields is relatively small), and its significance is clearly shown in Fig. 1 as the ragged pattern superimposed to the smooth contribution from $f(p)$. We note that the contribution of the correction term $\epsilon(y)$ appears stronger for the blue plates, while the result shown in Fig. 1 is representative of that for the other passbands.

The third CCD field (at the very edge of the Schmidt plates) was left out of the calibration, and the corresponding list of photometric standards was used only as reference catalog for the external comparisons (sec. 6.1).

The post fit errors of unit weight, σ_0, after elimination of the outliers (convergence was always reached in less

[2] That formula was made for Quick-V plates, but is a good approximation for POSS I and, by assumption, for POSS II plates.

Table 4. Precision of the transformations to linear magnitudes

Plate	*function*	*No. of standards*	σ_0 (mag)
N321	$V_{12} = t(v, y)$	45	0.117
64-O	$O = t(b, y)$	43	0.091
64-E	$E = t(r, y)$	41	0.127
XP442	$R_P = t(r, y)$	40	0.075
XJ442	$J = t(b, y)$	43	0.068

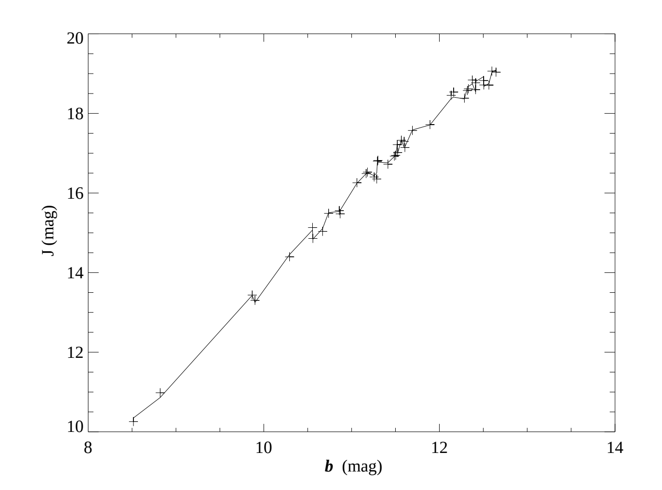

Fig. 1. Plate XJ442: calibration of the instrumental photometric index b to the linearized magnitude J. The line connects the computed values $J = J(b, y)$ for the CCD standards (crosses)

than 4 iterations), are presented in Tab. 4 for each of the five Palomar plates used.

4.4. Inverse transformations.

The derivation of photographic magnitudes and colors in the Johnson-Cousins system from the sets of *natural* magnitudes requires the inversion of the transformations to the natural bandpasses discussed above (see Tab. 3).

We have chosen to express the color transformations directly as $(O - V_{12}) \rightarrow (B - V)$, $(V_{12} - E) \rightarrow (V - R_c)$ for the POSS I pair, and as $(J - V_{12}) \rightarrow (B - V)$, $(V_{12} - R_P) \rightarrow (V - R_c)$ for the POSS II pair. This provides us with two determinations of the standard colors $B - V$ and $V - R_c$, although the two solutions are partially correlated because of the common V_{12} plate. The POSS II + Quick-V solution yielded a simple linear transformation from $J - V_{12}$ to the standard color $B - V$, as expected from the linear relations $V_{12} = V_{12}(V, B - V)$ and $J = J(B, B - V)$ in Tab. 3. The mean error of unit weight of the transformation (shown in Fig. 2) is 0.15 mag. The residuals as function of V and $B - V$ do not contain any significant systematic pattern as shown in Fig. 3. The transformation to $V - R_c$ did require corrective terms in the natural color $J - V_{12}$; this resulted in a final error of 0.1 mag and negligible systematics.

The transformations derived using the POSS I pair have properties in all similar to those just described. A linear function in $O - V_{12}$ provided a systematically clean calibration to $B - V$ with a precision of better than 0.1 mag. The *red* calibration resulted in a similar precision; but, besides the linear term in $V_{12} - E$, it required terms up to the second order in $O - V_{12}$ to clean the residual systematic errors. This is probably due to the coarse initial approximation $E \simeq R_c$.

Finally, standard V magnitudes were derived inverting the linear relation in Tab. 3, i.e., $V = V_{12} + 0.15(B - V)$. Values from both solutions gave, as expected, highly correlated values of V magnitudes ($|\Delta V| \leq 0.02$ mag), as there is only one V_{12}, and the two $(B - V)$'s (which are themselves correlated) carry only a 15% weight.

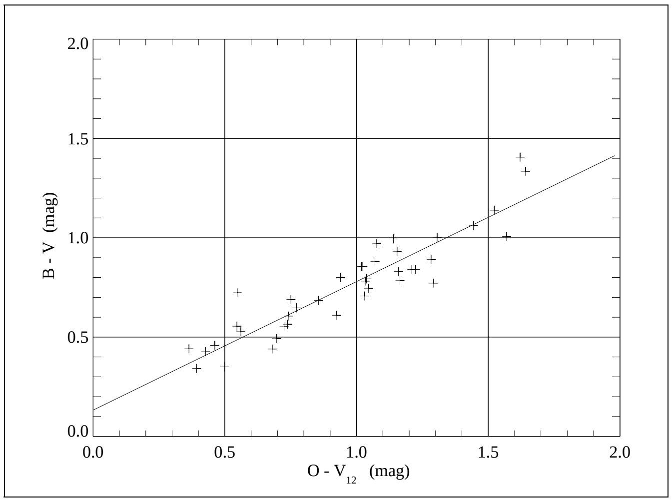

Fig. 2. Plates N321 and 64-O: color transformation for $(B-V)$

4.5. The final catalog of magnitudes and colors

The transformations just described yield standard magnitudes and colors (V, $B - V$, and $V - R_c$) for all measured objects. Also, the solutions based on POSS I plates can be directly compared to those obtained via POSS II plates, thus providing us with the means for a thorough assessment of their relative internal accuracy. However, before merging the two solutions for improved precision, particular attention was devoted to the characterization and the elimination of residual systematic errors.

4.5.1. Relative systematic residuals

The relative systematic differences $\Delta(B - V)$ as function of plate position for both the POSS I and the POSS II photometry are shown in Fig. 4 (*left*); each element therein

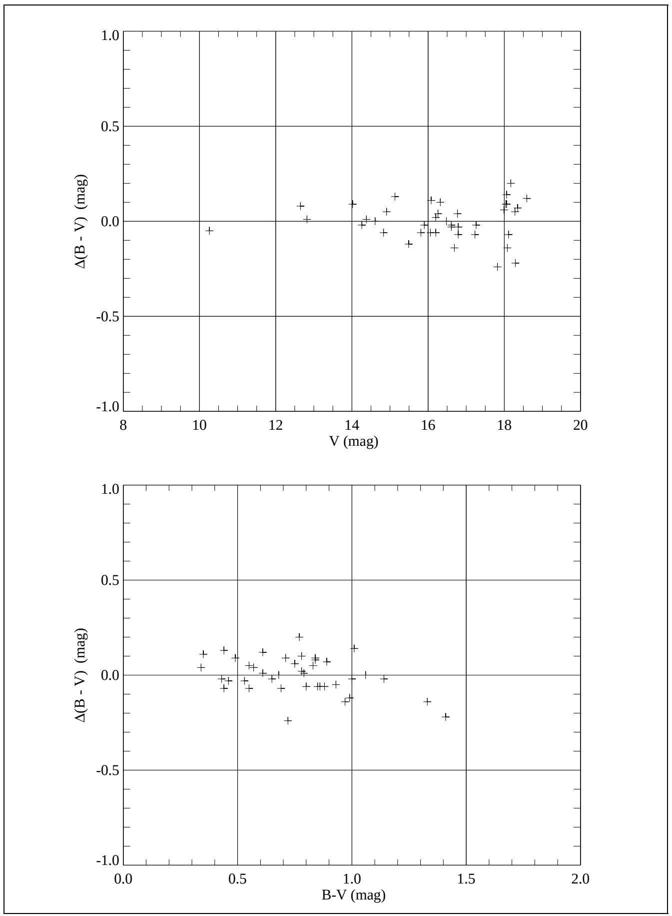

Fig. 3. Plates N321 and 64-O: residuals of the $(B-V)$ transformation versus V (top) and $(B-V)$ (bottom)

contains the average of the difference $(B-V)_I-(B-V)_{II}$ for all stars in an area of 200×200 pixels. The grey-scale is between -0.3 mag (black) and $+0.3$ mag (white), and the differences peak at 0.5 mag. A similar behaviour, although smaller in amplitude, exists but is not plotted for $V-R_{\rm c}$ (maximum at 0.3 mag) and for V [peak smaller than 0.1, as systematics are $0.15\Delta(B-V)$, see previous section].

The photometric solutions utilized to produce Fig. 4 were previously corrected for vignetting (see discussion above) and for the y-gradient derived in Sect. 4.3. Therefore, Fig. 4 demonstrates the existence of residual systematic differences.

The method adopted for the evaluation and the removal of those systematic residuals is based on a simple least squares fitting procedure, in which the photometry from one of the two solutions is "flattened" onto that of the other solution. Preliminary comparisons with external photometric catalogs (see Sect. 6 below) established that the POSS II-based photometry is the main source of the residual systematic variations. Therefore, the residuals map on the left panel of Fig. 4 is to be interpreted as the table of the raw corrections to the POSS II photometry. Least squares fits to this map, and to similar ones for ΔV and $\Delta(V-R_{\rm c})$, provide the bi-dimensional scalar fields, $S_{(B-V)}(x,y)$, $S_V(x,y)$, and $S_{(V-R_{\rm c})}(x,y)$, used for the actual correction of the POSS II photometry. The correction $S_{(V-R_{\rm c})}(x,y)$ required a fourth order polynomial, $S_{(B-V)}(x,y)$; and $S_V(x,y)$, a fifth order polynomial. The *central* panel in Fig. 4 shows the empirical correction model $S_{(B-V)}(x,y)$, and the *right* panel shows the residuals after model subtraction.

4.5.2. Final averaging

The previous subsection has detailed on the procedure adopted for homogenizing the photometries obtained from the two different plate sets. Here, we address the integration of these photometric data to improve precision.

The limiting magnitude of the survey is imposed by the Quick-V plate (N321), which is a few magnitudes brighter than the POSS I and POSS II plates. Therefore, for the entire interval covered by this survey ($9.5<V<18.5$), magnitudes in the final catalog are calculated as the plain average of the POSS I values and the corrected POSS II values. Objects with photometric indices from only one plate set are listed with the corresponding standard photometry. Also, for stars bluer than $B-V=0.3$, we list the POSS II $B-V$ in order to avoid extrapolation of the POSS I color transformation outside the boundaries of the original calibration.

Finally, the photographic data were corrected for a residual offset, $\Delta(B-V)=-0.04$, calculated from independent photometric data of Harris & Upgren (1964), Slettebak et al. (1961), Doinidis & Beers (1990, 1991). The external comparison of the final photometry is presented in Sect. 6.

5. Astrometry

The second fundamental task of data reduction is the astrometric calibration of the plates, the various steps of which are presented here.

5.1. Plate-plate transformation

In order to take advantage of the potentially high precision of the *relative* positions, it is necessary to define an accurate coordinate transformation between the positions of the program objects on an arbitrary plate to their positions on the reference plate.

It is well known that Schmidt plate astrometry is affected by various systematic effects related to geometric distortions, magnitudes, and colors. The causes may be:

1. *instrumental*: produced by the physical bending of the plates, and by the optical aberrations of the telescope, as well as stresses in the photographic emulsion and scanner irregularities;

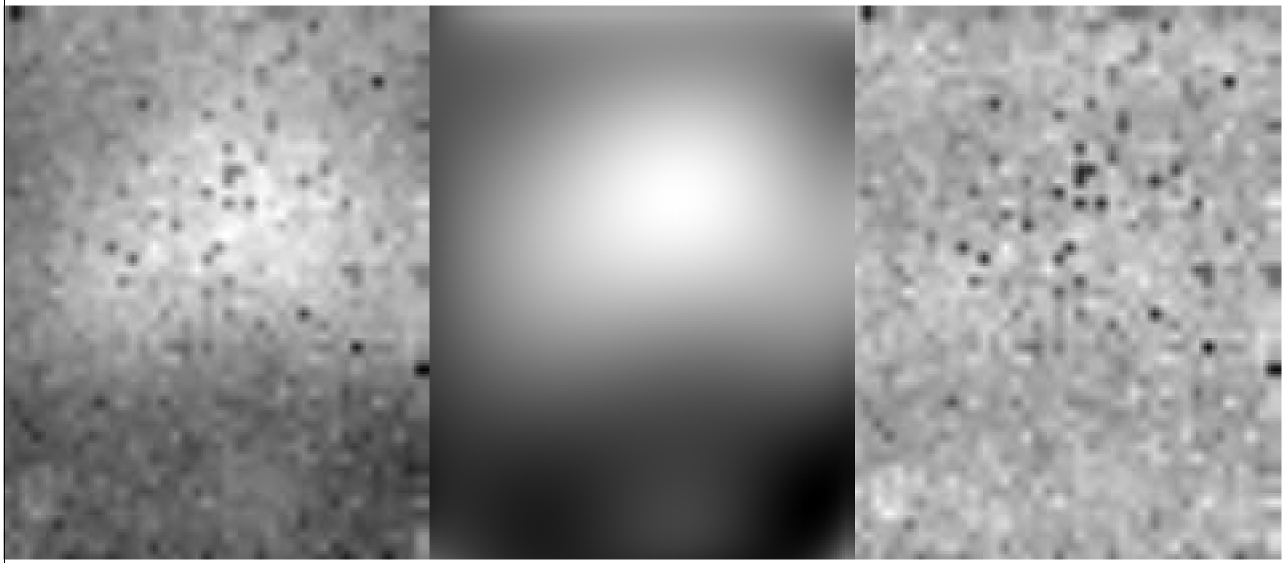

Fig. 4. NGP. Spatial systematic $\Delta(B-V)$ between POSS I and POSS II photometry: $\Delta(B-V)$ original map (*left*); model (*center*); original map after model subtracting (*right*)

2. *observational*: deriving from differential atmospheric refraction, and from the variability of the refraction coefficient as a function wavelength, resulting in color effects;
3. *astrophysical*: relating to errors in the transformation originating in intrinsic correlations between proper motions with position, magnitude, and color.

Naturally, the instrumental and observational effects should be corrected for by the calibration procedures, while care must be devoted in order to preserve the astrophysical effects which are the goal of this kind of studies.

5.1.1. Reference stars

A coordinate transformation is defined by a set of reference objects that are generically assumed as "fixed points". In general, reference stars with homogeneous kinematics and low intrinsic velocity dispersion would suffice (e.g. star clusters).

Galaxies provide an ideal reference set, because they materialize directly the *quasi*-inertial (absolute) reference frame. However, galaxies are difficult to use as direct calibrators in the astrometric solution, both for astronomical reasons, i.e., dense catalogues of galaxies with good positions do not exist, and for technical one related essentially to (1) a low spatial density at the limiting magnitude of this survey and to (2) centering problems on extended images. To avoid these disadvantages, we pursued the classical technique of selecting low-proper-motion reference stars[3] for the definition of the coordinate transformation. Such a transformation forces the reference stars to have zero *mean* proper motion, while the extragalactic objects then have result with a false *apparent* mean motion which can be removed as the final step of the reduction.

Following this second approach, we selected reference stars in the magnitude range $16 < V < 17.5$; this provides at least 180 stars degree^{-2}, well-distributed on the plate.

5.1.2. Subplate-overlap method

The conversion of plate-coordinates, (x_n, y_n) (with $n = 2, \ldots, N$), to the corresponding coordinates, (x_1, y_1), on the reference plate has been implemented using cubic[4]

[3] A proper motion solution directly based on the measurable galaxies was indeed attempted. The results did show a decreased precision as a consequence of increased centering error. However, the transformation constants were quite close to those derived with the traditional, statistically better behaved, solution.

[4] The choice of the polynomial degree is related to the 3$^{\rm rd}$ order geometric distortion deriving from the spherical deformation of Schmidt plates in the ideal case of elastic deformation and in absence of optical aberrations.

polynomials of the form:

$$x_1 = f(x_n, y_n; \boldsymbol{a}) = \sum_{i=0}^{3}\sum_{j=i}^{3} a_{ij}\, T_i(x_n)\, T_j(y_n) \quad (3)$$

$$y_1 = g(x_n, y_n; \boldsymbol{b}) = \sum_{i=0}^{3}\sum_{j=i}^{3} b_{ij}\, T_i(x_n)\, T_j(y_n), \quad (4)$$

where T_i is Chebyshev's polynomial of i-th order and the vectors $\boldsymbol{a}$ and $\boldsymbol{b}$ contain the 10 + 10 coefficients of the transformation. The coefficients are determined via a least squares best-fit to the set of reference stars, iteratively identifying (and rejecting) outliers. Using Chebyschev polynomials instead of standard ones does *not* improve the final accuracy of the transformation[5]. However, these polynomials are numerically more efficient, especially because the significance of each term can be easily evaluated.

The problem of the geometric distortions in Palomar Schmidt plates has been investigated by Taff et al. (1990) and by Lattanzi and Bucciarelli (1991); these works clearly showed that standard plate models present significant geometric residuals with a correlation-length of $\sim$ 0.5-1 degrees. For this investigation, we adopt, from the several techniques developed to correct for such distortions, a method similar to the *overlapping subplates* described in Taff (1989) and successfully implemented in Taff et al. (1990). We divided the field in 4×5 subplates of about 1 degree square. For each subplate a coordinate transformation of the form of eqs. (3)-(4) was derived by means of an iterative least squares procedure based on reference stars distributed over an area *larger* than the actual subplate used for the program stars. This is similar to the technique of Reid (1990), and the expanded frame is about 25% larger in linear size than the subplate. This expansion is introduced to (1) avoid the extrapolation of the polynomial functions at the subplate edge, and (2) improve the analytical continuity of the transformations between adjacent subplates.

In Fig. 5 the residuals of the XP442-to-N321 transformation are presented for the case of a global function (*left*) and for the 4×5 subplates solution (*right*). Each vector represents the average of the fit-residuals, $(\Delta x, \Delta y)$, for the reference stars in a square of $\sim$ 400 $\times$ 400 pixels ($1''.7$/pixel). The largest residual for the global solution reaches $0''.43$, and stream-like systematic distortions are clearly visible, while the subplate solution shows randomized residuals, the largest of which is less than $0''.26$. An alternative procedure to the subplate method is the use of a global high order transform (see e.g. Ojha et al. 1994ab, Bienaymé 1993).

Table 5 presents the errors of unit weight of the various coordinate transformations. The higher accuracy of POSS II transformations derives from the better sampling of the low granularity emulsions and also from the shorter time baselines.

[5] See also Soubiran (1992a) who adopted Legendre's polynomials.

Table 5. Internal accuracy of the transformations (4×5 subplates). Reference plate N321 (V_{12})

Plate	Band	Pixel (arcsec)	ΔT (year)	σ_x (arcsec)	σ_y (arcsec)
64-O	O	$1.70''$	-33.018	0.25-0.36[a]	0.20-0.27
64-E	E	1.70	-33.018	0.25-0.34	0.22-0.29
XJ442	J	1.00	$+6.932$	0.09-0.13	0.08-0.12
XP442	R_p	1.00	$+6.788$	0.10-0.13	0.08-0.12

[a] The two values are the minimum and maximum among twenty different subplate solutions.

5.2. Relative proper motions

After projecting the positions of all of the program objects onto the frame of the reference plate (N321), the relative proper motions are directely computed via the linear model,

$$x(t) = x_0 + \mu_x\,(t - t_1) \quad (5)$$
$$y(t) = y_0 + \mu_y\,(t - t_1), \quad (6)$$

where t_1 is the reference plate epoch, (μ_x, μ_y) are the proper motions in the plate-coordinates frame, and (x_0, y_0) are the re-computed positions at the epoch t_1. Annual parallax is not included in Eqs. (5)-(6) because the observations are generally taken at the same period of the year; in any event, the effect is negligible for the typical distances (a few Kpc) of the stellar sample.

The proper motion errors, σ_{μ_x} and σ_{μ_y}, result from the covariance matrix of the solution. Obviously, the error is dependent on the precision of the various positions, σ_{x_i}, σ_{y_i} $(i = 1, \ldots, N)$, which depends, in turn, on the centering error, and, for the secondary plates, on the accuracy of the plate-to-plate transformations. However, the actual precision is dominated by that of the positions at the two extreme epochs, as the errors decrease inversely with the time baseline, $\Delta T = t_{\rm Max} - t_{\rm min}$.

In Fig. 6, the total internal error $\sigma_\mu = \sqrt{\sigma^2_{\mu_x} + \sigma^2_{\mu_y}}$ is plotted versus the magnitude V. The expected magnitude effect is clearly visible. For $V \leq 17$ mag, $\sigma_\mu \approx 2.5$ mas/yr; and the mean error increases with magnitude as reported in Tab. 6.

Magnitude- and color-dependent effects on proper motions are a concern as they would have to be disentangled from possible cosmic effects, which, in turn, are crucial to establish astrophysically important correlations. The details of our analysis of possible photometry-induced systematic errors in the astrometric reduction leading to the proper motions are discussed in full in Spagna et al. (1996b). There, we selected several hundred stars (the astrometric members of the open cluster STOCK2) with an

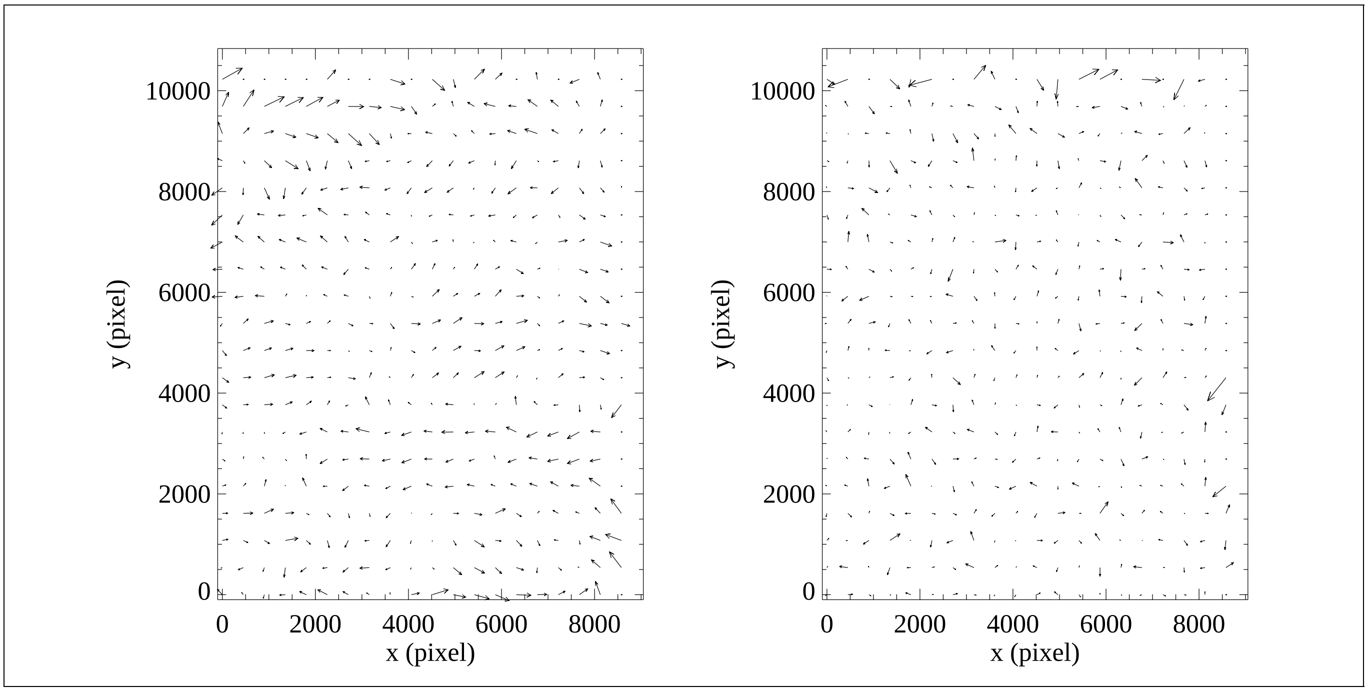

Fig. 5. Geometric distortions. Residuals of the XP442-N321 transformation for a global function (*left*), and for a 4×5 subplates solution (*right*)

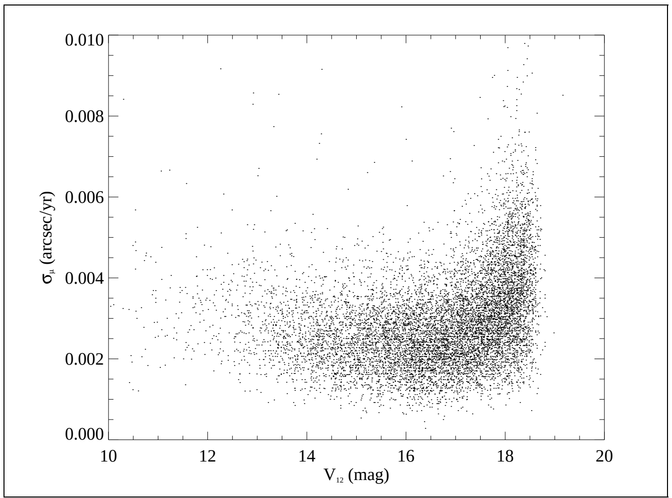

Fig. 6. Total internal error, σ_μ, of proper motions

internal kinematics coherent within 0.5 mas/yr, and their proper motions were correlated with V and $(B-V)$.

A regression analysis yielded magnitude-dependent (V) terms smaller than 0.1 mas/yr mag^{-1} , and color-dependent $(B-V)$ terms smaller than 1 mas/yr mag^{-1}. These values can be considered small and the corresponding systematic effects are neglected also in this work.

Before the conversion to absolute proper motions, the relative motions, μ_x, μ_y, were oriented onto the equatorial frame, $\mu_\alpha \cos\delta$[6] , μ_δ, via a simple rotation of the x-y axis. Note that an overall rotation valid throughout the area surveyed is only an approximation of the real transformation; a rigorous model should require a local rotation at each (x, y). We can estimate the systematic distortion of this approximation by means of the formula: $\phi \simeq 0.5 \arccos(\sin^2\delta_f \, \cos\Delta\alpha_f + \cos^2\delta_f)$, where $\Delta\alpha$ and δ_f are the range in R.A. and the declination of the whole field, while ϕ is the largest deviation from the mean rotation. We find $\phi \simeq 1\overset{\circ}{.}1$. Then, the resulting systematic effect on proper motions is less than $\sin\phi = 0.02$ of the total motion μ, so that for $\mu \lesssim 0.1$ arcsec/yr we have systematic errors below 2 mas/yr.

Table 6. Mean total errors, $\langle\sigma_\mu\rangle$, for magnitude intervals

V (mag)	No. stars	$\langle\sigma_\mu\rangle$ (mas/yr)
9.5-11	29	6.43
11-12	94	5.06
12-13	215	3.51
13-14	539	2.75
14-15	940	2.51
15-16	1372	2.50
16-17	2024	2.52
17-18.5	5017	3.35
Total	10230	

[6] Hereafter μ_α for brevity.

5.3. Absolute proper motions

The survey contains about 700 objects classified as "galaxies". This sample includes misclassified objects (e.g. unresolved double stars and faint objects). Thus, a *reliable* subsample of 520 galaxies for the establishment of the absolute reference frame was selected on the basis of their "kinematics", i.e. rejecting outlier and objects with large errors.

The absolute proper motions were then derived from the equations

$$\mu_\alpha^{(\mathrm{abs})} = \mu_\alpha - \mu_\alpha^{(\mathrm{gal})} \quad (7)$$

$$\mu_\delta^{(\mathrm{abs})} = \mu_\delta - \mu_\delta^{(\mathrm{gal})}, \quad (8)$$

where μ_α and μ_δ are the relative proper motions described in the previous paragraph, and $\mu_\alpha^{(\mathrm{gal})}$, $\mu_\delta^{(\mathrm{gal})}$ are the *apparent* mean galaxy motions. Strictly speaking, $\mu_\alpha^{(\mathrm{gal})}$ and $\mu_\delta^{(\mathrm{gal})}$ are position-dependent, but here they were approximated with their averages of the whole set. In Table 7 the actual values of mean and dispersion are reported.

Table 7. Relative "motions" of the reference galaxies: average and dispersion

	average	*dispersion*
$\mu_\alpha^{(\mathrm{gal})}$	+5.5 mas/yr	3.9 mas/yr
$\mu_\delta^{(\mathrm{gal})}$	+5.7 mas/yr	4.0 mas/yr

In Fig. 7, the *Vector Point Diagram* (VPD) is presented. The asymmetric distribution in Fig. 7 is consequence of the stellar asymmetric drift, as we will discuss in Sect. 9.2.

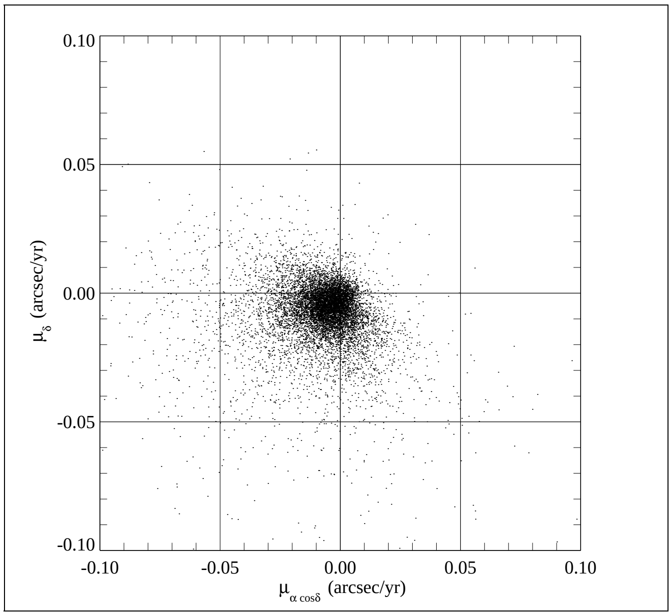

Fig. 7. Vector point diagram (VPD)

6. External comparisons

In order to check the data reduction procedures, comparisons to independent catalogs were performed on the photometric and astrometric results.

6.1. Photometric tests

Photographic NGP photometry was compared with photoelectric V and $B-V$ of a sample of BD stars in the magnitude range $9.5 < V < 12.0$ mag published by Harris & Upgren (1964) and Slettebak et al. (1961), claiming an accuracy of $\sigma \lesssim 0.01$ mag. In the range $12 < V < 15$, comparison data with similar accuracy are from Doinidis & Beers (1990, 1991). Photometry in the range $13.5 < V < 18.5$ was also tested utilizing CCD V, $(B-V)$ and $(V-R_c)$ data ($\sigma \lesssim 0.05$ mag) from the third CCD field, which was excluded from the photographic calibration. This CCD field, being situated on the North-West edge of the plates, is very useful for checking on geometric systematic effects.

The statistics of the differences ΔV, $\Delta(B-V)$ of our photographic catalog minus the photoelectric and CCD photometry are presented in Table 8; the individual differences are plotted in Figs. 8-9: *crosses* are for the bright photometric standards of Harris & Upgren (1964) and Slettebak et al. (1961), *diamonds* for the intermediate photometry of Doinidis & Beers (1990, 1991), and *triangles* for our CCD standards.

Table 8. Statistics of the external photometric tests

V	ΔV		$\Delta(B-V)$	
Range	Average	RMS	Average	RMS
9.5-12	0.026	0.094	-0.026	0.128
12-15	0.043	0.073	0.031	0.092
15-18.5	-0.019	0.103	0.027	0.201

The mean dispersion (RMS) is a reliable indicator of the precision of the photographic solution, because (except for $V \gtrsim 18$ mag) it is dominated by the photographic error. Excluding outliers above 3 σ (some of which are candidate variable stars) and for $V < 18$ mag, the photographic error appears close to 0.1 mag for both V and $B-V$, as reported in Tab. 8. Note that the large RMS for $\Delta(B-V)$ in the faintest bin (V =15-18.5) depends on the larger error of the CCD photometry at $V > 18$; infact for $15 < V < 18$ the RMS of $\Delta(B-V)$ is only 0.11 mag. The RMS of $\Delta(V-R_c)$, computed from all the available CCD standards in the range $13.5 < V < 18.5$, is 0.15 mag, which decreases to 0.06 mag for $V < 18$ mag.

The mean values provide information on the *external* accuracy of the photographic solution. The presence of (possibly magnitude-dependent) biases of a few hundredths of magnitude are evident in both colors.

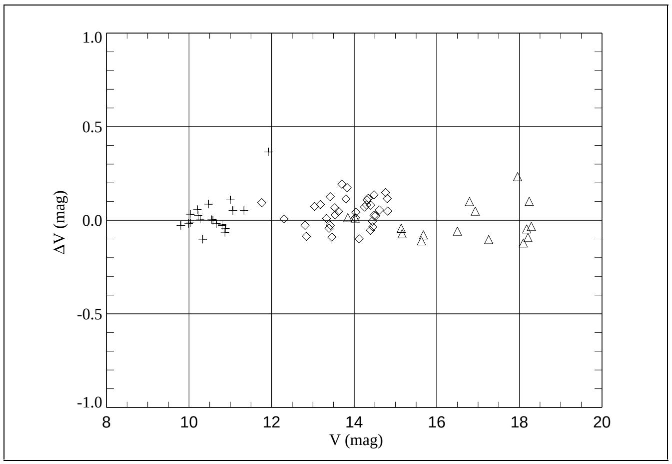

Fig. 8. ΔV differences in the sense photographic minus photoelectric (*crosses* and *diamonds*, see text) and photographic minus CCD (*triangles*)

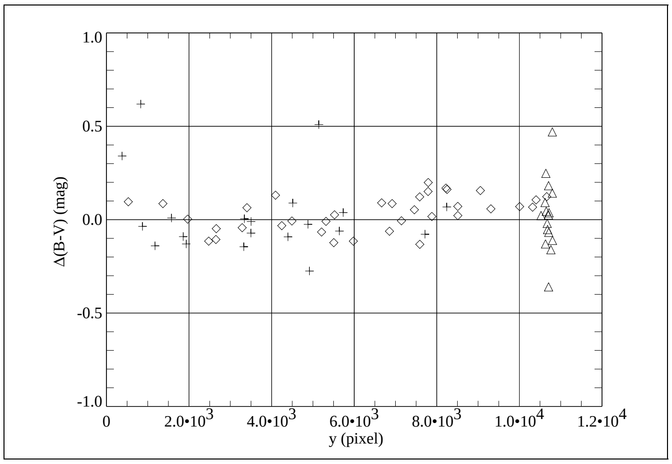

Fig. 9. $\Delta(B-V)$ differences versus y_1 (pixel). The *crosses* and *diamonds* (represent differences in the sense photographic minus photoelectric photometry, respectively for bright and intermediate standards (see text); the *triangles* represent photographic–CCD photometry differences

Concerning the geometric effects, the presence of significant residual geometric errors is excluded on the basis of the available data. The photoelectric standards that are distributed on the whole field show local variations of about 0.1 mag, but do not determine large scale effects. In Fig. 9, the $(B-V)$ differences are plotted versus the y_1 coordinate, and no significant geometric trend is evident. (Note that the outliers close to ±0.5 mag are very faint or bright stars.)

Systematic effects have also been investigated by means of the technique proposed by Bienaymé et al. (1992). In the hypothesis that the color distributions are constant within the NGP field, the averages of the photographic $(B-V)$ and $(V-R_c)$ values have been computed for the stars with $13 < V < 16.5$ on a grid of 8×10 squares of $0\overset{\circ}{.}5$ on a size. The results are two random maps, with a RMS of the average colors of a few hundredths of magnitude, 0.06 and 0.04 mag for $B-V$ and $V-R_c$, respectively.

6.2. Astrometric comparison with Lick NPM catalog

The Lick Northern Proper Motion (NPM) program (Klemola et al. 1987) is a survey of 300 000 stars ($8 < B < 18$) providing photometry $[B,\ (B-V)]$ and absolute proper motions with respect to 50 000 galaxies. Recently, Klemola et al. (1993) have published the first part of a catalog, NPM1, covering the regions outside the galactic plane. The astrometric accuracy is quoted as $\sigma_{\alpha,\delta} \simeq 0\overset{\prime\prime}{.}15$ for positions, and $\sigma_\mu \simeq 5$ mas/yr for proper motion components.

The NGP and NPM1 proper motions have been compared via a transformation which converts the NGP components from the J2000 equatorial frame to the B1950 frame adopted in the NPM1 catalog. We utilize a scale sensitive rotation-translation, whose four parameters have been determined via a best-fit to a set of 61 common stars selected in the magnitude range $12 < V < 16$ mag and with NGP proper motion errors < 5 mas/yr. The resulting error of unit weight was $\sigma_0 \simeq 6.0$ mas/yr in each component, which is consistent with the internal precision quoted in both catalogs.

As expected, no significant scale change was detected ($< 1\%$), while an offset $\Delta\mu_\alpha \simeq -4.3\pm0.9$ mas/yr is apparent, revealing a systematic rotation between the NGP and NPM1 frames. We estimate that the contribution to this μ_α shift from the uncertainty in the NGP absolute frame is only ~ 1.2 mas/yr.

7. Star-counts and completeness

In Fig. 10 the V star-counts are presented and compared with different surveys. The solid histogram shows the normalized counts (deg^{-2} mag^{-1}) from our survey, while the dotted histograms show the $\pm1\sigma$ confidence interval in the case of poissonian noise. This distribution derives from the photometric catalog of 12 708 stars within the 20 degrees squared region studied.

The agreement with the data of Stobie & Ishida (1987) (*diamonds* in Fig. 10) is quite good down to $V \simeq 18.5$, although we underestimate their counts below $V = 12$ mag, mainly because of identification problems on bright saturated images. However, the M3 data (*crosses*) from Soubiran (1992b) are systematically higher at the faint magnitudes compared to the other two surveys. This can be (partially) explained with the lower latitude of the M3 field.

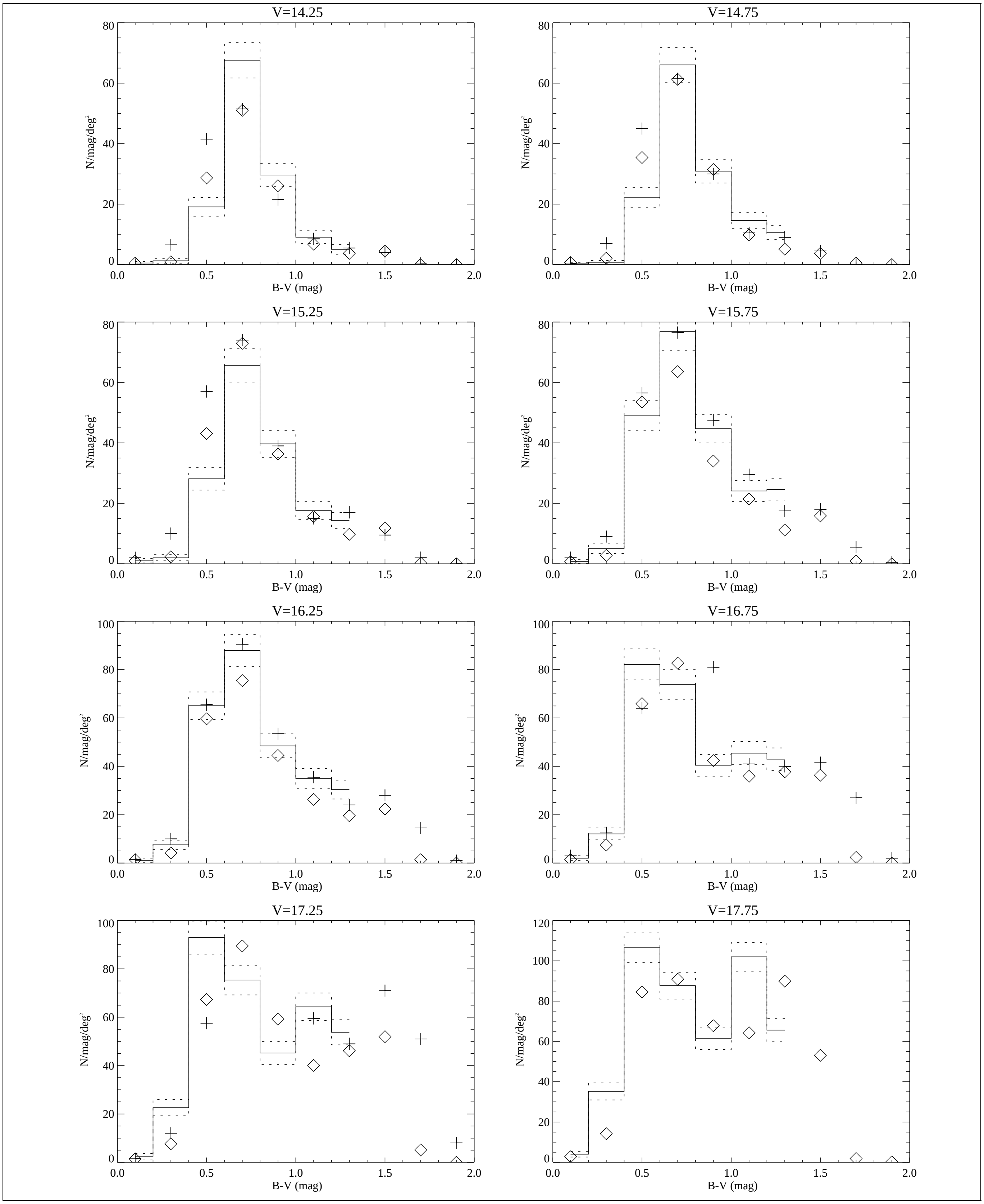

Fig. 11. Comparison of our $B-V$ distributions (*histogram*) at various magnitude intervals with those of Stobie & Ishida (*diamonds*) and Soubiran (*crosses*)

Table 9. Color-magnitude star-counts within 19.9 squared degrees

V	$B-V$ (mag)															Tot.
(mag)	0.05	0.15	0.25	0.35	0.45	0.55	0.65	0.75	0.85	0.95	1.05	1.15	1.25	1.35	1.45	
9.75	0	0	0	0	1	1	2	3	3	2	0	1	1	1	0	15
10.25	1	0	1	2	1	3	2	2	2	2	2	2	0	1	1	22
10.75	0	1	4	4	5	10	3	3	2	5	2	1	0	0	0	40
11.25	1	1	3	2	11	6	9	7	9	10	7	0	1	3	0	70
11.75	0	1	3	1	7	18	15	17	14	10	3	2	4	0	0	95
12.25	0	0	0	0	8	17	45	27	14	22	8	5	0	1	0	147
12.75	0	0	0	3	9	37	55	47	39	25	7	4	2	1	0	229
13.25	1	1	0	4	3	40	101	80	37	30	8	9	7	4	1	326
13.75	0	2	0	1	12	43	98	85	71	31	24	8	9	6	0	390
14.25	1	1	1	4	14	62	120	149	79	39	20	16	10	10	5	531
14.75	1	0	1	2	17	71	145	118	79	44	30	28	27	15	9	587
15.25	2	2	3	5	25	87	134	127	89	69	37	33	26	31	7	677
15.75	1	2	3	17	48	147	192	114	103	75	54	42	55	43	12	908
16.25	2	2	4	26	100	159	190	160	107	86	65	74	76	45	8	1104
16.75	3	5	12	36	130	197	168	126	79	82	90	91	119	52	14	1204
17.25	3	7	17	73	179	191	173	127	85	95	94	162	149	65	7*	1427
17.75	4	12	31	109	209	215	198	151	111	134	161	245*	208*	53*	3*	1844
18.25	9	22	56	140	245	221	210*	201*	186*	262*	356*	332*	154*	31*	4*	2429

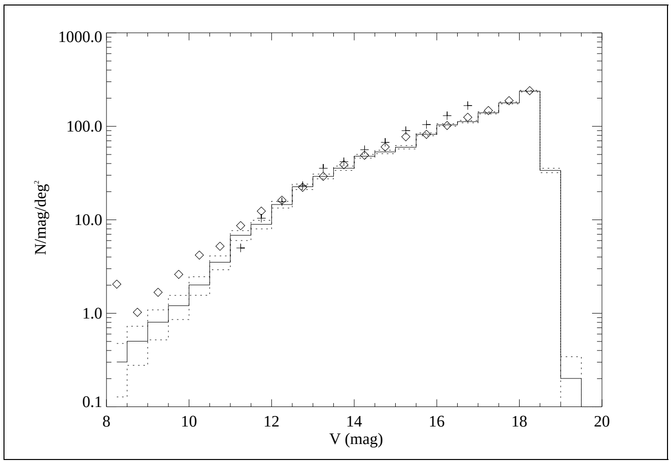

Fig. 10. Comparison of our V star-counts (*histogram*) with those of Stobie & Ishida (*diamonds*) and Soubiran (*crosses*)

Table 9 reports the star counts for magnitude intervals in the calibrated color range $0 \leq (B-V) \leq 1.5$ mag. The asterisks mark the incompleteness region of the photometric catalog for $B \gtrsim 19$ mag. The $(B-V)$ color distributions are plotted in Fig. 11 as a solid histogram and compared with the data of Stobie & Ishida (1987) (*diamonds*) and Soubiran (1992b) (*crosses*). The dotted histograms show the $\pm 1\sigma$ poissonian error.

The distributions are similar, although a few significant differences are noticeable expecially at faint magnitudes.

8. Structure and kinematics

8.1. Distance determination

Stellar distances have been estimated by means of the the distance modulus, $V - M_V$, and a given relation $M_V = f(B-V)$ for main sequence stars. The problems with such an evaluation, as remarked for example by Kuijken & Gilmore (1989), are:

- the presence of stars not belonging to luminosity class V, essentially giants and subgiants, whose distances are systematically in error;
- the contamination of unresolved double stars, which produce a distance underestimation of up to a factor $\sqrt{2}$ for pairs of same magnitude and luminosity class;
- the interstellar extinction, which, if ignored, leads to distances larger than real;
- the dependence of the $M_V(B-V)$ relation on the chemical composition, which typically tends to overestimate the distance of low metallicity stars (e.g. subdwarfs).

In the direction perpendicular to the galactic plane the interstellar extinction can be reasonably neglected. On the other hand, double stars are more of a problem for Schmidt plates because of the larger scale factor. The overall effect depends on the frequency of binary systems and on the distribution of the magnitude difference, Δm, of the components. These distributions are known for Population I stars, for which Dunquennoy & Mayor (1991) claim a 50% binary fraction, but are not well determined for Population II stars, for which only a lower limit of about 20-30% can be set (Carney 1983). However, Kroupa et al. (1993) suggest that binary components are sampled independently from the mass function, so that the mean effect is greatly reduced. In the next steps the contamination of unresolved double stars is neglected.

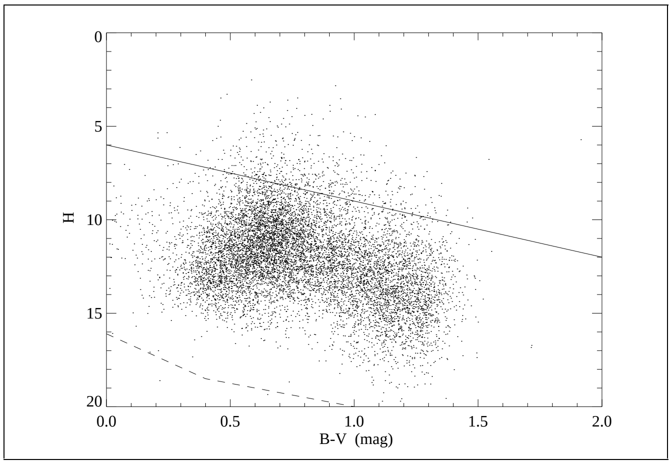

Fig. 12. Reduced proper motions diagram

As far as the presence of evolved stars is concerned, an exact solution cannot be applied if spectroscopic observations or photometric indicators of gravity are not available. On similar data sets, previous authors adopted a classification based on a-priori probability of the various population models (Chiu 1980), while Majewski (1992) and Ohjia et al. (1994a, 1994b)) neglected the presence of evolved stars. Soubiran (1992b) and Kharchenko et al. (1994) utilized an intermediate procedure in order to identify and exclude the more evident evolved stars; this is what we implemented for our survey. This method is based on photometric and kinematic data as combined in the quantity H (*reduced proper motion*), which, in the definition of Luyten (1922), reads

$$H \equiv V + 5\,\log\mu + 5 = M_V + 5\,\log T - 3.378 + A_V \qquad (9)$$

H relates the peculiar tangential velocity T (km/s) and absolute magnitude M_V to the observed apparent magnitude V (mag) and total proper motion μ (arcsec/yr). A_V (mag) is the extinction in the visual passband, neglected in the NGP direction. Figure 12 gives the H vs. $B-V$ diagram. The solid line separates the region dominated by main sequence stars from the area where giants are predominant (with a contamination of bright low-proper motion dwarfs), while the dashed line is the "bright" limit to the white dwarfs region. Both ridge lines are from Soubiran (1992b). Figure 12 also shows the typical bimodal distribution of $B-V$ produced by nearby red stars and more distant blue stars.

Finally, the metallicity effect has been statistically accounted for by means of the procedure suggested by Kuijken & Gilmore (1989), which assumes a vertical metallicity gradient of $\partial\,[\mathrm{Fe/H}]\,/\partial z \simeq -0.3\ \mathrm{Kpc}^{-1}$. The correction ΔM_V to the Hyades color-magnitude relation, as given by Laird et. al (1988), can be written as

$$M_V \simeq 5.64\,(B-V) + 1.11 + \Delta M_V[\delta_{0.6}(Fe/H)] \qquad (10)$$

where $\Delta M_V(\delta_{0.6})$ is expressed as a function of the normalized ultraviolet excess $\delta_{0.6}$, whose relation with the iron abundance is provided by Carney (1979) in the form

$$\delta_{0.6} \simeq -0.0776 + \sqrt{0.01191 - 0.05353\ [\mathrm{Fe/H}]} \qquad (11)$$

Starting from a solar metallicity approximation ($\Delta M_V = 0$) a first distance d_0 is established, and used to derive a new [Fe/H] approximation which provides a new ΔM_V and a new distance. The process is iterated until convergence is reached.

The uncertainty on *individual* distances has been estimated at 26%, taking into account the photometric accuracy ($\sigma_V \simeq \sigma_{(B-V)} \simeq 0.1$ mag). This value does not include uncertainties on the $M_V(B-V)$ relation, contaminations from binaries, subgiants and giants, and errors on individual metallicity corrections.

8.2. Velocity

The (U, V, W) components of the linear velocity (Km/s) in the galactic reference frame[7] are related to the proper motions, μ_α and μ_δ, and to the radial velocity, v_r, via the transformation:

$$\begin{bmatrix} U \\ V \\ W \end{bmatrix} = \boldsymbol{G}(\alpha,\delta)\cdot \begin{bmatrix} 4.74\,d\,\mu_\alpha\cos\delta \\ 4.74\,d\,\mu_\delta \\ v_r \end{bmatrix} \qquad (12)$$

where d is the distance in parsec and $\boldsymbol{G}(\alpha,\delta)$ is the matrix defining the local rotation to the galactic frame (see e.g. Murray 1983). Equation (12) represents a local projection of the velocity vector, which depends on the right ascension and declination of the given star. Neglecting the position dependent term $\boldsymbol{G}(\alpha,\delta)$ results in systematic distortions of about 2% (cf. Sect. 5.2).

For instance, at the center of our field, the transformation matrix is

$$\boldsymbol{G}(\alpha_c,\delta_c) = \begin{bmatrix} 0.849\,732 & -0.524\,015 & -0.057\,990 \\ 0.525\,655 & 0.850\,532 & 0.016\,804 \\ 0.040\,517 & -0.044\,762 & 0.998\,176 \end{bmatrix} \qquad (13)$$

As the radial velocity is unknown, we cannot estimate the W component. On the other hand, as apparent from the third column of $\boldsymbol{G}$, reliable U and V velocities are derived directely from the proper motions; residual uncertainties on both components are smaller than $\sim 6\%$ and 2% of v_r, respectively.

Error propagation gives a typical relative error on each component of the linear tangential velocity, $\sigma_v/v = \sqrt{(\sigma_d/d)^2 + (\sigma_\mu/\mu)^2}$, below 30% for $\mu > 10$ mas/yr.

[7] We adopt the triad that defines U as the velocity component, relative to the solar motion, toward the galactic center, V along the rotation direction, and W as the component perpendicular to the galactic plane.

9. Discussion

9.1. Spatial distribution

In order to study the stellar density perpendicular to the galactic plane, we have to understand the statistical properties of the photometric parallax catalog derived from our magnitude-limited ($V \lesssim 18.5$ mag) survey. The stellar sample includes 9721 stars, selected by means of the reduced proper motion diagram, in the color range $0.3 \leq (B-V) \leq 1.3$. The size of this sample results from (1) the sample volume increasing with distance ($\Delta V \propto z^2 \Delta z$), and (2) the exponential decrease of the stellar density with z (which depends on the spectral type).

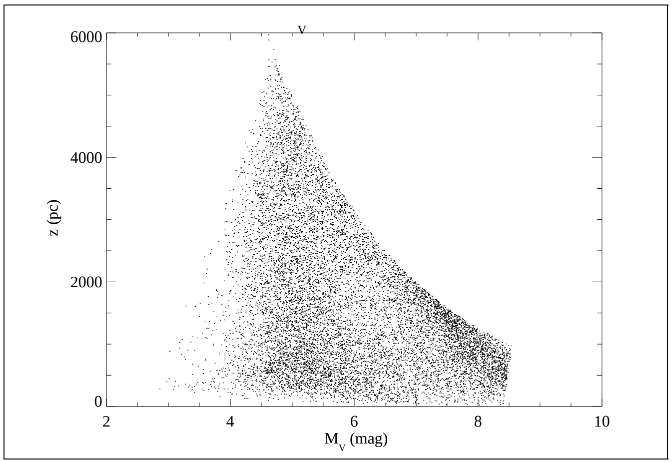

Fig. 13. Distance distribution vs. M_V

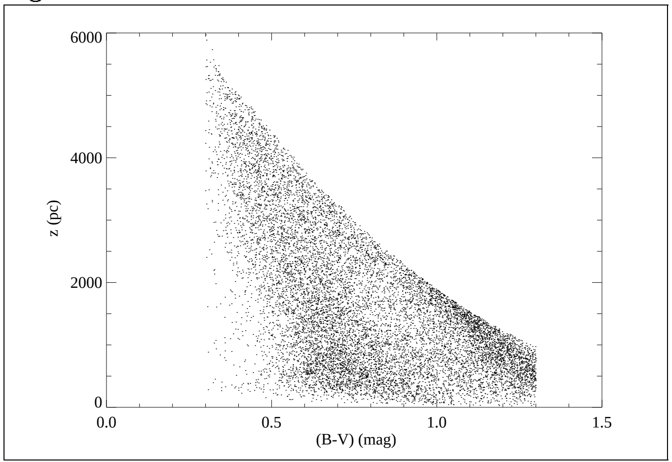

Fig. 14. Distance distribution vs. $(B-V)$

Moreover, at larger distances the redder (faint) stars cannot be observed because of the limit $V = 18.5$ mag. In Fig. 13, the distribution of the height, z (pc), above the plane is plotted against absolute magnitude M_V. Note the sharp limit in distance, which depends on stellar brightness and, except for the Malmquist bias, sets the completeness of the survey. The lack of brighter stars ($M_V \lesssim 4.5$ mag) at large distances is an indicator of galactic structure and age of the outer populations. For comparison, the distribution of z versus the observed $(B-V)$ is shown in Fig. 14; the low mean metallicity at large distance ($z > 2$ Kpc) is responsible of the presence of bluer stars.

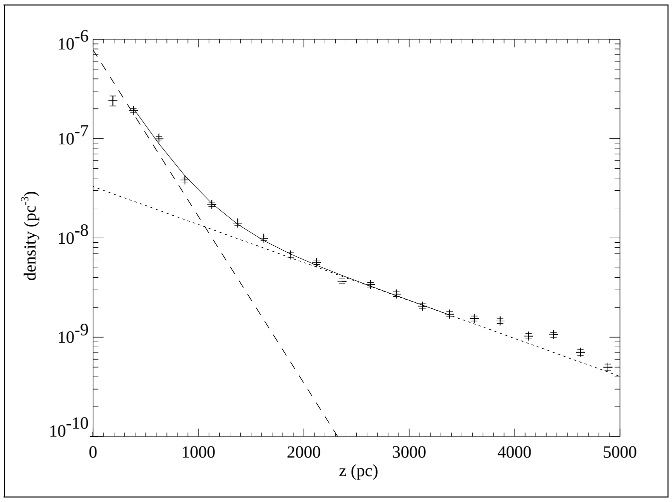

Fig. 15. Density distribution perpendicular to the galactic plane for stars within $4.5 \leq M_V \leq 5.0$ mag

Finally, in Fig. 15 the density distribution (stars per pc^3) is presented as a function of distance, z (pc). We selected a subsample of 2292 stars in the absolute magnitude range $4.5 \leq M_V \leq 5.0$ as a tracer of the density distribution, up to $\simeq 5$ kpc (cf. Fig. 13), Each point represents the mean density in a bin of 250 pc; the error bars are square root values of the corresponding density. The first bin (0-250 pc) is probably affected by the loss of stars brighter than $V = 12$ mag, and has not been included in the next analysis[8]. The density at $z > 4500$ pc is affected by the turn-off of the old, metal deficient, populations.

The density in the range $250 < z < 4500$ pc has been compared with a two-component law of the form:

$$\rho(z) = \sum_{n=1}^{2} \rho_{0n}\, \mathrm{e}^{-z/z_{0n}}, \tag{14}$$

where $n = 1, 2$ refers to the thin and thick disk, respectively. The halo has not been directly included in the density model, as the star counts in the z-range considered are insufficient to separate a third component clearly, although the presence of halo stars can be inferred indirectly

[8] Another factor contributing to the reduced number counts in the first bin (compared to an exponential density law) is that a function with a continuous density gradient, e.g., $\rho(z) \propto \mathrm{sech}^2\,(z/2z_0)$ (van der Kruit & Searle 1981), is more appropriate as $z \to 0$ pc.

from the analysis of the results obtained with the model in Eq. (14).

Best fits in the range $250 < z < 4500$ pc yield a reduced Chi-squared, χ^2/ν, of $\simeq 0.3$; however, the solutions of the fit *vary* with the selected distance range. In particular, the scale height of the thick disk decreases sensibly when the upper z-limit is lowered. For $z_{\rm max} = 4500$ pc, we obtain $h_{01} \simeq 285 \pm 10$ pc, $h_{02} \simeq 1378 \pm 51$ and $\rho_{02}/\rho_{01} \simeq 1/31$. For $z_{\rm max} = 3500$ pc the parameters *converge* to:

$$\rho_{01} = (7.8 \pm 0.8)\, 10^{-7}\ \mathrm{pc}^{-3} \tag{15}$$

$$z_{01} = 259 \pm 12\ \mathrm{pc} \tag{16}$$

for the thin disk parameters, and

$$\rho_{02} = (3.3 \pm 0.4)\, 10^{-8}\ \mathrm{pc}^{-3} \tag{17}$$

$$z_{02} = 1137 \pm 61\ \mathrm{pc} \tag{18}$$

for the thick disk, which implies a ratio $\rho_{02}/\rho_{01} \simeq 1/23$. This solution also minimizes the reduced Chi-square ($\chi^2/\nu \simeq 0.25$), and the parameters do *not* vary if $z_{\rm max}$ is further reduced. We explain this effect as due to the contamination of halo stars, which increases the counts for $z \gtrapprox 3500$ pc, thus raising the scale height of the thick disk. Therefore, the values in Eqs. (15)-(18) should be reliable estimations of the parameters of the thin and thick disk.

9.2. Kinematics

Kinematical properties have been analyzed with a subsample of 6844 stars (70% of the whole kinematic sample) having accurate total proper motions ($\sigma_\mu < 3.5$ mas/yr). This sample is representative of the observed population within the imposed constraints $0.3 \leq (B-V) \leq 1.3$, and $V \leq 18.5$ mag.

In Fig. 16, the U and V velocities with respect to the Sun are plotted versus z. The symmetry of the U component around $\langle U \rangle \approx 0$ is clear, signifying that the Galaxy is not expanding nor contracting. The different behaviour of the V component, with an excess of negative velocities, is directly related to the stellar *asymmetric drift*, i.e., the rotational lag of the populations with larger dispersions.

Mean values and dispersions of the velocities distributions are reported in Table 10 for distance intervals of 250 pc. The corresponding errors are $\sigma/\sqrt{n}$ for the averages, and $\sigma/\sqrt{2n}$ for the dispersions, with σ the sample standard deviation. The medians, $\tilde{U}$ and $\tilde{V}$, are also included. The mean values, $\langle U \rangle$ and $\langle V \rangle$, and their errors, $\sigma_{\langle U \rangle}$ and $\sigma_{\langle V \rangle}$, are shown in Fig. 17 against the $\langle z \rangle$ of each bin. The diamonds represent the $\tilde{V}$ medians.

As expected, $\langle U \rangle \simeq$ const, while $\partial \langle V \rangle / \partial z < 0$ *indicates* the asymmetric drift. Moreover, we notice that the mean velocities extrapolated toward $z \to 0$ are not null. The stars closer than $z \sim 750$ pc yield $\langle U \rangle_0 \approx -10$ Km/s, while a straight line fit gives a zero-point value of ≈ -20 Km/s for $\langle V \rangle$. This effect is the reflection of the peculiar motion of the Sun with respect to the mean motion of the stellar sample analyzed. These results agree with the basic solar motion $u_\odot \simeq 9.9$ Km/s and $v_\odot \simeq 17.7$ Km/s published by Delhaye (1965) for local F-M dwarfs.

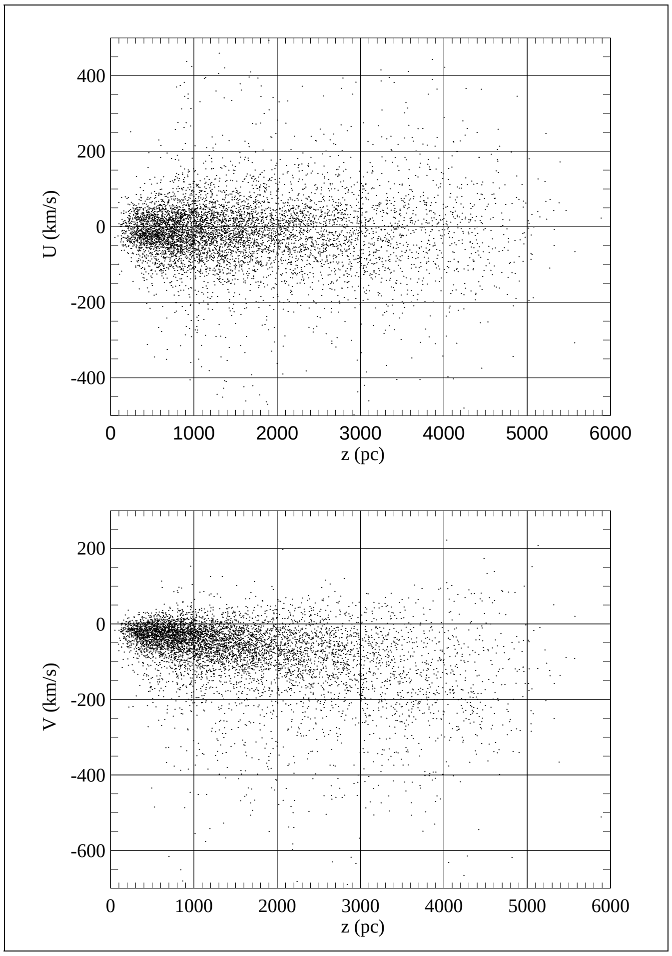

Fig. 16. Dispersion of the U (*top*) and V (*bottom*) velocities with distance, z (pc), perpendicular to the galactic plane

In Fig. 18, the $\langle V \rangle$'s of Tab. 10 are plotted versus σ_U^2 for $z \leq 2500$ pc. The solid line represents the relation

$$\langle V \rangle = -v_\odot - K\, \sigma_U^2 \tag{19}$$

first observed by Strömberg (1924) for the solar neighborhood. For $v_\odot$ in Eq. (19), the peculiar solar velocity with respect to the local standard of rest (LSR), we adopted the value of +10.5 Km/s (Penston et al. 1969); and for K the value of 1/120 Km/s^{-1} given in Binney & Tremaine (1987, p.198). Equation (19) can be derived from axially symmetric dynamical equations at $z = 0$, together with a few assumptions on the correlations among the velocity dispersions, the orientation of the velocity ellipsoids, and the mass distribution of the disk (cf. Gilmore et al. 1989). Figure 18 confirms that the bins corresponding to nearby

Table 10. First and second moments of U and V (Km/s) with z. Distance bins are 250 pc apart. $\tilde{U}$ and $\tilde{V}$ are median values

z_{max} (pc)	$\langle z \rangle$ (pc)	N	$\langle U \rangle$ (Km/s)	$\tilde{U}$ (Km/s)	$\langle V \rangle$ (Km/s)	$\tilde{V}$ (Km/s)	σ_U (Km/s)	σ_V (Km/s)
250	189.1	134	-6.7 ± 3.8	-8.1	-26.3 ± 2.7	-19.1	43.9 ± 2.7	30.8 ± 1.9
500	390.4	643	-14.2 ± 1.9	-16.3	-34.5 ± 1.6	-27.3	49.3 ± 1.4	40.1 ± 1.1
750	625.2	875	-15.4 ± 1.9	-16.1	-38.3 ± 1.8	-29.4	57.3 ± 1.4	51.8 ± 1.2
1000	869.6	880	-10.0 ± 2.9	-12.8	-48.4 ± 2.3	-36.1	85.8 ± 2.0	67.9 ± 1.6
1250	1120.1	722	-9.9 ± 3.6	-7.7	-60.7 ± 2.9	-44.6	97.4 ± 2.6	79.2 ± 2.1
1500	1372.6	566	-24.6 ± 4.3	-20.3	-70.0 ± 3.7	-54.3	101.6 ± 3.0	87.9 ± 2.6
1750	1621.9	524	-9.3 ± 4.3	-10.6	-83.5 ± 4.1	-64.8	98.7 ± 3.0	92.7 ± 2.9
2000	1869.5	392	-7.4 ± 5.8	-9.3	-91.5 ± 5.5	-66.1	114.7 ± 4.1	109.3 ± 3.9
2250	2121.6	364	-15.2 ± 5.0	-8.6	-101.0 ± 6.3	-77.6	96.2 ± 3.6	119.7 ± 4.4
2500	2363.4	308	-9.8 ± 5.2	-6.8	-97.9 ± 5.8	-80.9	91.5 ± 3.7	101.2 ± 4.1
2750	2625.1	286	-14.2 ± 6.0	-16.2	-102.8 ± 6.5	-81.6	101.0 ± 4.2	109.1 ± 4.6
3000	2868.0	222	-15.2 ± 8.1	-20.0	-111.1 ± 7.9	-85.5	121.4 ± 5.8	117.9 ± 5.6
3250	3116.3	196	-26.7 ± 8.4	-28.4	-128.8 ± 8.4	-104.0	117.3 ± 5.9	117.1 ± 5.9
3500	3376.6	178	-25.5 ± 9.4	-22.8	-130.9 ± 8.5	-117.7	125.4 ± 6.6	113.4 ± 6.0
3750	3615.1	132	-7.7 ± 13.0	-1.4	-166.3 ± 11.2	-156.1	149.2 ± 9.2	128.8 ± 7.9
4000	3865.6	128	6.1 ± 11.1	9.4	-160.0 ± 11.2	-142.3	126.1 ± 7.9	127.2 ± 7.9
4250	4120.9	100	-22.5 ± 14.6	-5.8	-143.2 ± 13.9	-131.3	145.9 ± 10.3	139.2 ± 9.8
4500	4372.3	84	-4.9 ± 13.5	-5.6	-153.7 ± 14.9	-180.6	123.8 ± 9.5	136.3 ± 10.5
4750	4618.4	46	11.7 ± 17.3	18.6	-122.7 ± 20.9	-118.6	117.1 ± 12.2	141.5 ± 14.8
5000	4861.7	34	-29.9 ± 21.9	-34.7	-155.3 ± 24.4	-125.3	127.7 ± 15.5	142.3 ± 17.3

stars (low σ_U) follow the model of Eq. (19). However, bins at larger distances do show a more complex asymmetric drift.

The velocity gradient $\partial\langle V\rangle/\partial z$ provides a quantitative measure of the vertical asymmetric drift. In the range $z \lesssim 2000$ pc, we derive a gradient of -40 Km/s Kpc^{-1}, which can be interpreted as an effect of the variation of the mixture of thin and thick disk stars at the various distances, as remarked by Soubiran (1993).

If we assume that thick disk stars *dominate* the sample (cf. Fig. 15) in the range $2000 < z < 3500$ pc, as Eqs. (15)-(18) suggest, we can investigate the z-dependence of the velocity ellipsoid of the thick disk. Murray (1986), Norris (1987), Hanson (1989) and Majewski (1992) claim a negative $\partial\langle V\rangle/\partial z$ ranging between 20 and 40 Km/s, while Soubiran (1993), Ojha et al. (1994ab), Robin et al. (1995) do not evidence any kinematical gradient in the thick disk. In Fig. 17, the $\langle V\rangle$ distribution does show a decreasing trend for $z > 2000$ pc; the calculated value is $\partial\langle V\rangle/\partial z \approx -15$ Km/s Kpc^{-1} for $2000 < z \leq 3000$ pc. For $z \approx 3500$ pc, a large variation of $\langle V\rangle$ is noticeable. It could be a consequence of a sudden variation of the thick disk characteristics, although it is more likely due to the presence of halo stars. The mean velocities are, in fact, more sensitive to the presence of a few high velocity stars than the mean density studied in the previous section.

To calculate a more reliable value for the asymmetric drift of the thick disk, we used the median, $\tilde{V}$, which is less sensitive to high velocity stars than $\langle V\rangle$, and it typically yields velocities 10-20 Km/s smaller. Within the interval $2000 < z \leq 3000$ pc, we get $-86 \lesssim \tilde{V} \lesssim -78$ Km/s, and a gradient of ~ -10 km/s kpc^{-1}. This finding, although confirming a negative gradient, tends to support the idea of a slow rate of change of the kinematical properties of the thick disk with z.

Figure 19 gives the velocity distributions in the (U, V) plane for stars in various distance intervals; and in Fig. 20, the marginal distributions of the V component are presented for the same bins.

Table 11. Parameters of the populations fitted to the V velocity distribution for $z < 3500$ pc

	Population	$\langle V\rangle$ (Km/s)	σ_V (Km/s)	*fraction*
1.	Thin disk	-32 ± 1	30 ± 1	31%
2.	Thick disk	-81 ± 4	66 ± 3	45%
3.	Halo	-225 ± 22	143 ± 9	24%

The observed (U, V) distributions are the sum, convolved with the velocity errors, of the distributions of the various structures (thin disk, thick disk and halo) weighed according to their local number density. These distributions may be described, in a first approximation[9], as Schwarzschild's (gaussian) velocity ellipsoids.

[9] Gaussian velocity ellipsoids can represent the kinematics of the disk only in the solar neighborhood and for age-selected sets of stars (cf. Mihalas and Binney 1981, chap. 7). Away from the plane, the proper dynamical assumptions would no longer apply. Also, evolutionary effects, like diffusion processes (e.g. the Spitzer-Schwarzschild mechanism), tend to modify the ve-

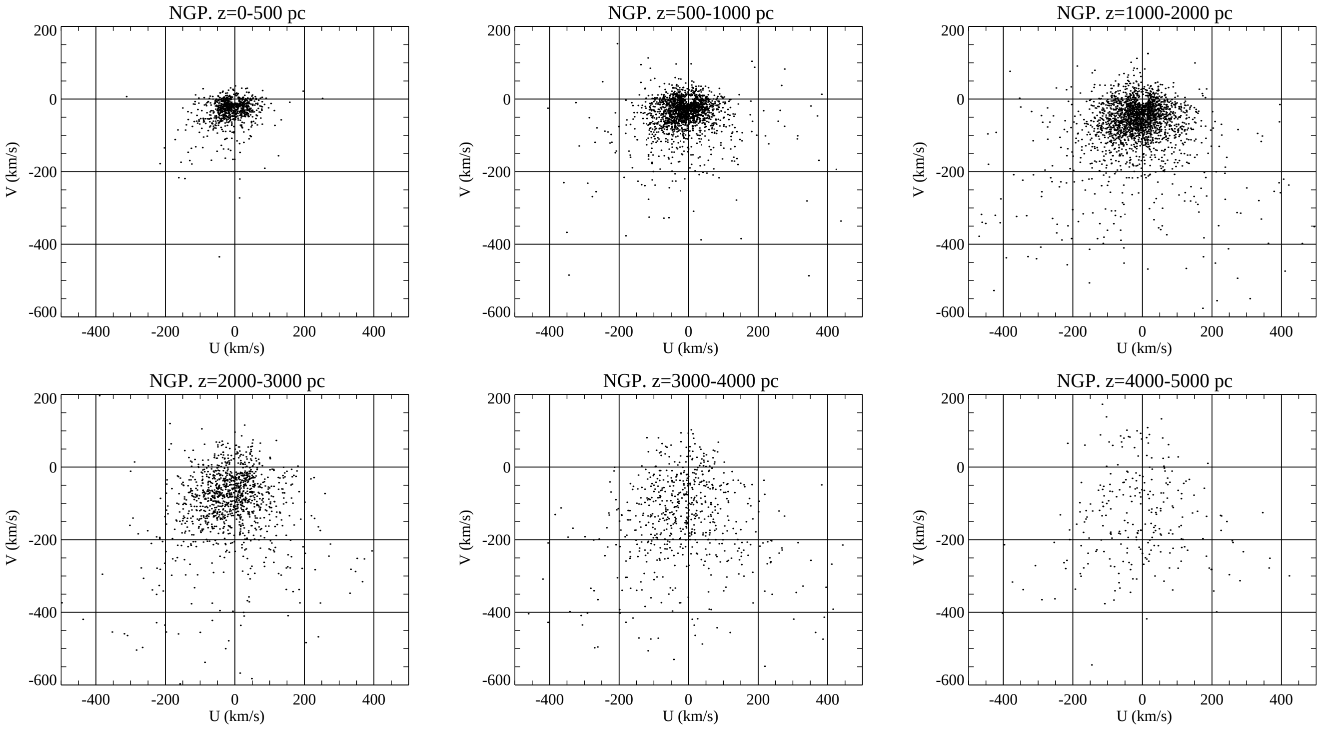

Fig. 19. Velocity distributions on the (U, V) plane at different distance intervals

In Fig. 21 the distribution of the V component for 6290 stars having distances $0 < z < 3500$ pc is shown and compared with a best-fit kinematical model (dashed line) consisting of the sum of the three populations, thin disk, thick disk and halo. The single gaussian distributions are plotted as solid lines, and their parameters are reported in Table 11. The reduced Chi-squared ($\chi^2/\nu = 1.3$) indicates that the fit is statistically compatible with the data with a confidence level $\alpha = 0.95$. [Note that a two-population model ($\chi^2/\nu = 5.65$) must be rejected with a confidence level of 0.9999.]

The interpretation of such a result must be qualified by the following considerations: first of all, the gaussian functions are approximations of the real distributions. That could explain the excess of counts on the right side of the peak, which is produced by stars within a few hundred parsecs. This effect could be avoided adding another gaussian for such a low-dispersion component, or adopting a non-gaussian function with negative skewness for the thin disk. Second, the integration over a large range of distances, although improving the statistics, is sensitive to z-dependent variations of the kinematics and relative density of the various populations, as well as to contaminations of different components because of the increasing errors. For example, in the region $z < 1500$ pc, dominated by the thin disk and by the low-dispersion component of the thick disk, we derive lower values of the asymmetric drift: $\langle V \rangle \simeq -22 \pm 1$ and -55 ± 7 Km/s respectively. Moreover, we emphasize that the observed velocity distribution is the convolution of the real distribution with velocity errors that, at a few Kpc, amount to several tens of kilometers per seconds; i.e., they are larger than the bin-size (20 Km/s in our case) and are comparable with the intrinsic dispersions, σ_U and σ_V, of the populations. This helps the gaussian approximation (and improves the goodness of the fit), but biases the computed parameters, in particular, overestimating the dispersions.

The distances of the stars contributing to the excess of counts to the right of the dashed curve in Fig. 21 (the sum of the three galactic components just discussed) are within few hundred parsecs from the Sun, as mentioned earlier. This would point to a "younger" (thinner) disk with little dispersion in the W-component of its galactic velocity, compared to a thin disk which evolution has started to

---

locity ellipsoid, increasing the U, V, W dispersions, and lagging the $\langle V \rangle$ with respect to the LSR.

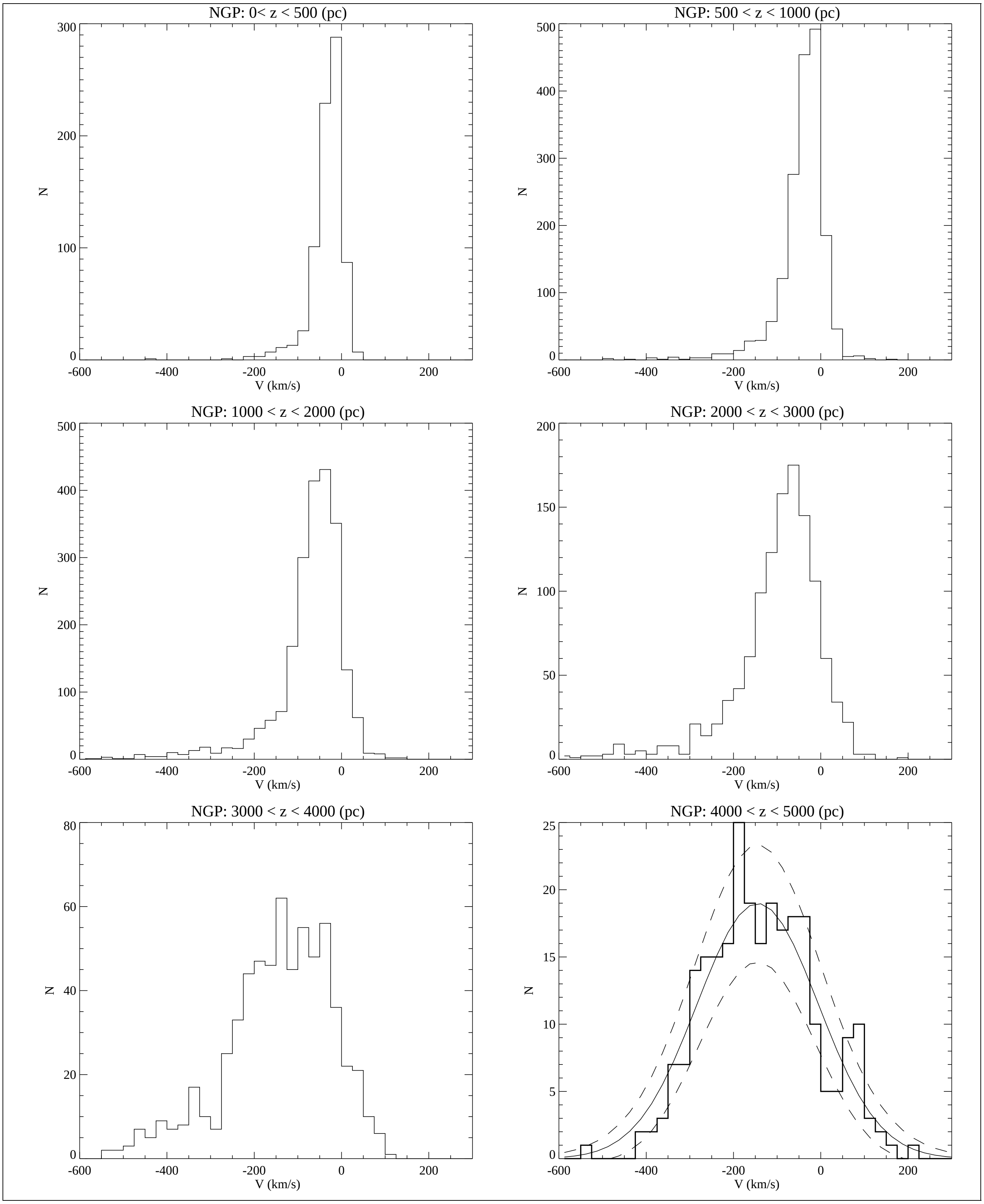

Fig. 20. V distributions at different distance intervals

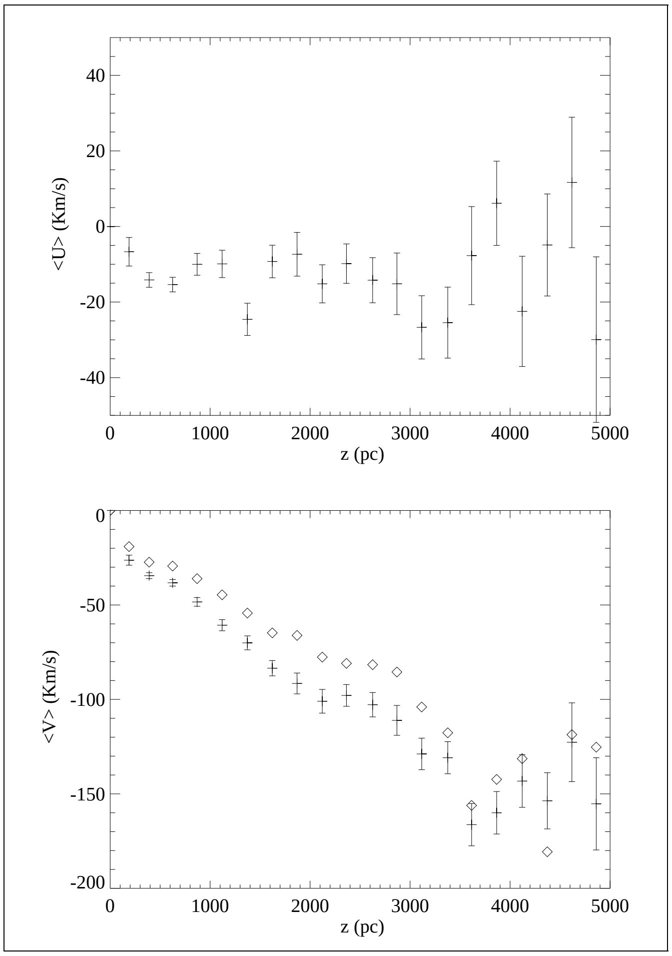

Fig. 17. Distribution of the mean U (*top*) and mean V (*bottom*) velocities with z (pc)

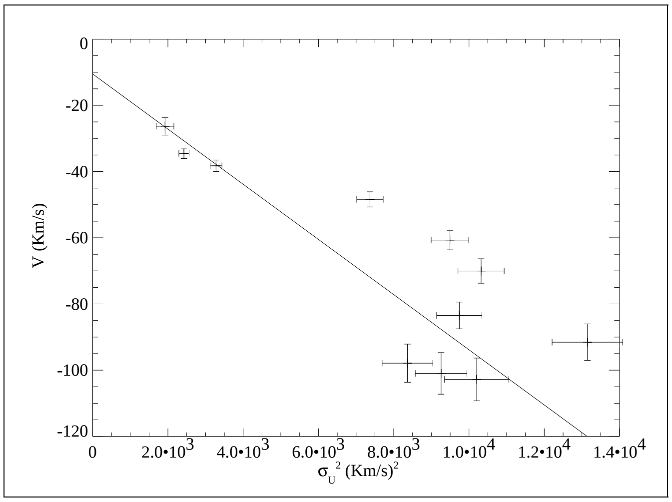

Fig. 18. Strömberg asymmetric drift. All stars with $z \leq 2500$ pc; bins are 250 pc in size

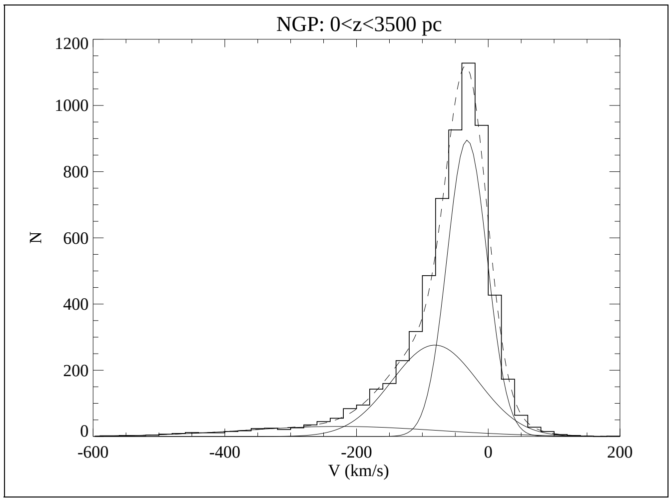

Fig. 21. Deconvolution of the velocity V distribution (*histogram*) for $z < 3500$ pc; the result of the fit is given as the gaussian functions (*solid lines*) used for the three standard populations; the *dashed line* represents the sum of the three components

slow down through heating processes (see also the last footnote). These mechanisms would then generate a vertical asymmetric drift in the thin disk (Soubiran 1993). Our simple deconvolution procedure is not adequate to properly address such a problem, which should certainly be investigated further, as it might contribute to a better understanding of the leading mechanisms governing the gravitational interactions within the thin disk.

We turn now our attention to the possible presence of peculiar structures in velocity space. Figure 19 presents several groups of stars away from the average locations of the various distributions. These sets could be interpreted as kinematical groups in the sense described in Majewski (1992) and Majewski et al. (1994). Specifically, we consider the excess of stars with $V > 0$ Km/s in the distance range $4000 \lesssim z \lesssim 5000$ pc. This is seen in the last panel of Fig. 20, which presents the V histogram of 264 stars with $4000 < z < 5000$ pc and $\sigma_\mu \leq 3.5$ mas/yr. The overall distribution is well modeled ($\chi^2/\nu \simeq 0.14$) by a gaussian function (shown as a solid line), with a mean of $\simeq -144.5 \pm 8.5$ Km/s and a standard deviation of $\simeq 138.7 \pm 6.0$ Km/s. The two dashed curves represent the 1-σ thresholds, assuming poissonian noise. The excess of stars in the velocity range 50-100 Km/s is significant at the 1-2 σ level, and it is confirmed for different constraints on the proper motion accuracy. On the other hand, as discussed before, it is reasonable to assume that the standard V distribution is asymmetric with negative skewness, as suggested also by the negative tail and by the sharp edge in the gap between 0 and 50 Km/s. In this case, the expected frequency of stars with $V > 0$ would be overestimated by the gaussian model, and, consequently, the peak at 50-100 Km/s would increase in significance.

This kinematically peculiar set contains 28 stars in the box $-200 < U < 200$ Km/s and $25 < V < 150$ Km/s, has a color range of $0.3 \lesssim B - V \lesssim 0.55$, and covers a magnitude range of $17.5 \lesssim V \lesssim 18.5$. Its mean distance is $\simeq 4400$ pc, and its dispersion $\simeq 270$ pc. The stars are distributed on the whole field, corresponding to a transversal extension of 500 pc at 4400 pc.

According to the typical photometric and astrometric accuracy, the expected error on individual stars is about 1000 pc on the distance, and 70 Km/s on each velocity components. If this excess of stars with positive V is not spurious, its physical interpretation could be:

– the brighter component of a more numerous kinematic group, not thermalized within the galactic populations;
– a chemical group at a lower height, whose distance and velocity have been overestimated because of a metallicity smaller than the mean local value set by the adopted fixed-gradient statistical model.

Further observations are necessary to investigate the actual nature of this sample (see below).

10. Conclusions

In this first paper of a series studying twelve regions along the meridian toward the Galaxy's anti-center, our objective has been to explore the phase space defined by the data, transformed with minimal use of modeling. A more sophisticated analysis, based for example on galactic models, is deferred to future work.

Our astrometry and photometry have been derived from three sky surveys made with the Palomar Schmidt, i.e., the POSS I, the POSS II, and the $\delta \geq 0°$ Quick-V. As this plate collection, digitized at the ST ScI, has the potential to produce the same kind of data over half the sky, the results of the present study are also a gauge of the scientific potential of these materials for more general studies of galactic structure.

We have derived colors and absolute proper motions for a magnitude limited sample (to $V = 18.5$) of about $1.3\ 10^4$ stars covering an area of 20 square degrees toward the North Galactic Pole. The calibrations show that, although precisions of 0.1 mag in the photometry and better than 3 mas/yr in the total proper motions are achieved, the most important aspect of obtaining scientifically critical data is the control of systematic errors. Photographic photometry appears to be particularly vulnerable to position-dependent systematics. Faint photometric standards, best if evenly distributed over the area studied, are essential; and we look forward to the eventual application of TYCHO data to this calibration.

Our data show quite clearly the presence of an extended (thick) disk population with a scale height of approximately 1 kpc. The halo is seen with an intrinsic velocity dispersion of ~ 140 Km/s, with respect to which the galactic disk at the Sun rotates with a speed of ~ 200 Km/s (assuming the halo is at rest). We confirm a vertical gradient of ~ -40 Km/s kpc^{-1} in the V-component of the velocity for $z \leq 2000$ pc, and find that the same V-component decreases with z at a rate of ~ -10 Km/s kpc^{-1} in the region $2000 < z < 3000$ pc, where the thick disk dominates. Assuming that it is the changing mixture of thin and thick disk stars the cause for the vertical gradient of the V-component of the galactic velocity, our results tend to depict a thick disk ($z > 2000$ pc) whose kinematics is slowly changing (if at all) with z.

Quite appealing is the possible discovery, described at the end of Sect. 9, of a kinematic group at an average distance of ≈ 4400 pc. The group contains 28 stars, all of which are fainter than $V \simeq 17.5$ mag. The stars are distributed within 1 kpc along the line of sight, and cover the entire extension of the field surveyed, i.e., ~ 500 pc. Given the large errors expected on individual estimates at large distances, caution is in order. Confirmation of the reality of this kinematic group and unraveling its nature require good spectroscopic data of adequate resolution or, alternatively (as radial velocities only good to ~ 15 km/s would suffice), a mixture of spectroscopy and improved photometry (including coverage of Johnson-Cousins U and/or I bands).

Several new POP I white dwarfs candidates (Fig. 12), intermediate age common proper motion pairs, and variable stars have been detected during this work. Follow-up work on these samples is planned but the necessary human resources are not currently available. Therefore, it is our intention to provide these data to anyone seriously interested.

Finally, we plan to release the whole NGP sample within six months of the publication of this article. Copies of the data will be sent to the data centers in Strasbourg (SIMBAD) and Greenbelt (NSSDC), and they will also be accessible via anonymous FTP at OTOAX2.TO.ASTRO.IT (193.205.67.42).

Acknowledgements. The authors are grateful to A. Ferrari for his continuing support of this program and of the collaboration between ST ScI and OATo. We are pleased to acknowledge S. Casertano for his many useful suggestions and comments which substantially improved earlier versions of this work, P.S. Bunclark for his contribution to the development of the early ST ScI plate processing software, and D. Rehner and L. Siciliano for their help with the PDS scans and the CCD data. We would like to acknowledge R. Morbidelli and M. Sarasso for their assistance in the management of the astronomical catalogs. Finally, we thank the referee, Pr O. Bienaymé, for his comments and helpful suggestions. This work has been supported in part by the Italian Ministry for Research (MURST). The ST ScI is operated by the Association of Universities for Research in Astronomy, Inc., under contract to NASA.

References

Bienaymé O., Mohan V., Crézé M., et al., 1992, A&A, 253, 389

Bienaymé O., 1993, A&A 278, 301
Binney J., Tremaine S., Galactic Dynamics, 1987, Princeton Univ. Press
Carney B.W., 1979, ApJ, 233, 211
Carney B.W., 1983, AJ, 88, 623
Chiu L.-T.G., 1980, ApJS, 44, 31
Delhaye J., Solar motion and velocity distribution of common stars, "Galactic Structure", 1965, eds. A. Blaauw & M. Schmidt, Chicago
Doinidis S.P., Beers T.C., 1990, PASP, 102, 1392
Doinidis S.P., Beers T.C., 1991, PASP, 103, 973
Dunquennoy A., Mayor M., 1991, A&A, 248, 425
Einasto J., Malyuto V.D., Kharchenko N.V., 1985, Astron. Circular No. 1394, 1
Evans D.W., 1988, PhD thesis, Cambridge
Gilmore G., Reid N., 1983, MNRAS, 202, 1025
Gilmore G., Wyse R.F.G., Kuijken K., 1989, ARA&A, 27, 555
Grøsbol P., Ponz D., 1985, Mem. S.A.It., 56, 429
Hanson R.B., 1989, BAAS, 192, 347
Harris III D.L., Upgren A.R., 1964, ApJ, 140, 151
Humphreys R.M., Landau R., Ghigo F.D., Zumach W., LaBonte A.E., 1991, AJ, 102, 395
Kharchenko N., Shilbach E., Sholz R.D., 1994, Astron. Nachr., 315, 4, 291
Klemola A.R., Jones B.F., Hanson R.B., 1987, AJ, 54, 501
Klemola A.R., Jones B.F., Hanson R.B., 1993, NSSDC/WDC-A-R&S, 93-41
Kroupa P., Tout C.A., Gilmore G., 1993, MNRAS, 262, 545
Kuijken K., Gilmore G., 1989, MNRAS, 239, 605
Laird J.B., Carney B.W., Latham D.W., 1988, AJ, 95, 1843
Landolt A.U., 1991, AJ, 104, 340
Aller L.H. et al., Landolt-Börnstein, vol. 2, subvol. b, 1982, eds. Springer-Verlag Berlin
L.Lanteri, 1996, in preparation
Lasker B.M., Sturch C.R., McLean B.J., Russell J.L., Jenkner H., Shara M.M., 1990, AJ, 99, 1613
Lasker B.M., 1992, Digital Optical Sky Survey, eds. H.T. MacGillivray and E.B. Thompson (Kluwer Academic Publishers, Dordrecht), 87
Lattanzi M.G., and Bucciarelli B., 1991, A&A, 250, 565.
Lattanzi M.G., 1993, Mem. S.A.It. 64, 1057
Majewski S.R., 1992, ApJS 78, 87
Majewski S.R., 1993, ARA&A, 31, 575
Majewski S.R., 1994, ApJ Lett., 427, 237
Mihalas D., Binney J., Galactic Astronomy, 1981, ed. Freeman and Company, S. Francisco
Mitton M., thesis, 1992, Turin
Murray C.A, Vectorial Astrometry, 1983, ed. Adam Hilger Ltd., Bristol
Murray C.A., Argyle R.W., Corben P.M., 1986, MNRAS 223, 629
Norris J., 1987, AJ, 93, 616
Ojha D.K., Bienaymé O., Robin A.C., Mohan V., 1994a, A&A 284, 810
Ojha D.K., Bienaymé O., Robin A.C., Mohan V., 1994b, A&A 290, 771
Penston M.V., Munday V.A., Penston M.J., 1969, MNRAS, 142, 355
Reid N., 1990, MNRAS, 247, 70
Robin A.C., Haywood M., Crézé M., Ojha D.K., Bienaymé O., 1995, A&A, in press
Russell J.L., Lasker B.M., Sturch C.R., McLean B.J., Jenkner H., 1990, AJ, 99, 1613
Slettebak A., Bahner K., Stock J., 1961, ApJ, 195
Soubiran C., 1992a, A&A 259, 394
Soubiran C., 1992b, Thèse de Doctorat de l'Observatorire de Paris
Soubiran C., 1993, A&A, 274, 181
Spaenhauer A., A Proper Motion Study in SA 57, 1989, proc. of "The Gravitational Force Perpendicular to the Galactic Plane", Danbury (Connecticut), 1989 19-20 May
Spagna A., PhD Thesis, Turin
Spagna A., Lattanzi M.G., Lasker B.M., McLean B.J, Massone G., 1996a, submitted to A&A Suppl.
Spagna A., Lattanzi M.G., Lasker B.M. McLean B.J, Massone G., Lanteri L., 1996b, in preparation
Stetson P.B., 1987, PASP, 99, 191
Stobie R.S., Ishida K., 1987, AJ, 93, 624
Straizys, Multicolor stellar photometry, 1992, Ed. Pachart Publishing House
Strömberg G., 1924, ApJ, 59, 228
Taff L.G., 1989, AJ, 98, 1912
Taff L.G., Lattanzi M.G., Bucciarelli B., 1990, ApJ, 358, 359
van der Kruit P.C., Searle L., 1981, A&A, 95, 105

This article was processed by the author using Springer-Verlag LaTeX A&A style file *L-AA* version 3.